High performance activated carbon anodes for supercapacitors for energy storage applications

Thomas Fone BEng

A Thesis

Submitted to the College of Engineering

Swansea University

In Fulfilment of the Requirements

For MSc in Materials Engineering by Research

08th September 2023

Engineering and Physical Sciences Research Council

Swansea University
Prifysgol Abertawe

Abstract

This work presents the optimisation of an activated carbon ink using Ethyl Cellulose as a binder for application as electrodes in supercapacitors. Effect of variation in the concentration of Ethyl Cellulose binder was explored adopting a commercially available Activated carbon as reference. The result was that the 10% EC concentration led to the best performance compared to the 20% and 5% EC inks, with a specific capacitance of 62.3F/g at 1.4A/g. It was hypothesised that the 20% EC ink had too much binder, potentially clogging up the pores in the activated carbon, while the 5% EC ink did not have enough binder, causing decohesion of the ink from the substrate, which severely limited the performance of the electrode. As part of the work, a special carbon provided by the sponsoring company was also tested using the same 10% EC recipe only substituting the new carbon instead of the commercial one. Particle size analysis of this carbon showed that the particles had a larger disparity of sizes compared to the commercial activated carbon. This new carbon gave a better result of 82.7F/g at 1.4A/g even with the particle size disparity.

Declarations

This work has not previously been accepted in substance for any degree and is not being concurrently submitted in candidature for any degree.

Signed.....[redacted].....

Date.....17/03/2023.....

This thesis is the result of my own investigations, except where otherwise stated. Other sources are acknowledged by footnotes giving explicit references. A bibliography is appended.

Signed....[redacted].....

Date.....17/03/2023.....

I hereby give my consent for my work, if relevant and accepted, to be available for photocopying and for inter-library loans **after expiry of a bar on access approved by the University.**

Signed..[redacted].....

Date.....17/03/2023.....

The University's ethical procedures have been followed and, where appropriate, that ethical approval has been granted.

Signed..[redacted].....

Date.....17/03/2023.....

Acknowledgements

I would like to thank my supervisors Prof Davide Deganello and Dr Chris Phillips for their continuous guidance, assistance and unstinting support. Without their assistance and encouragement this work would have been impossible to complete.

I would like to thank the sponsoring company the Enserv Group and in particularly Dr Aphidet Chasri for the industrial support.

I would like to thank Dr Daniel Jones for his efforts in enabling me to acquire the much-needed laboratory skills and also for sharing his knowledge and experience in electrochemistry.

Finally, I would like to thank my family, especially my parents, who have supported me throughout my education and have encouraged me to pursue my scientific interests.

Contents

CHAPTER 1: Introduction

1.1 Background: Energy challenge

Supercapacitors are an energy storage component with a very high specific power compared to the regular battery architecture as the energy in a supercapacitor is stored in surface reactions between the electrode material and ions within the electrolyte. One downside with supercapacitors is that they do not have a comparatively low specific energy compared to regular batteries. One of the largest uses for supercapacitors currently is as high input and output storage in electric vehicles [1], for example they are used in regenerative breaking which collects the energy needed to decelerate the vehicle quickly, then stores this energy in supercapacitors which can then be used to accelerate the vehicle. However, there are still areas of interest that supercapacitors have increased potential in such as in bulk energy storage for grid scale applications [2].

Current energy production systems are keeping up with the demand of electricity needed grid wide. However, many of the production sources use the combustion of fossil fuels and non-renewable materials to create energy which damages the environment by creating carbon dioxide, which is a current problem due to it being a greenhouse gas which prevents reflected infrared solar rays leaving the atmosphere which in turn contributes to global warming. These energy production sources also create other pollutants such as sulphur dioxide which all cause damage to the environment. As well as damaging the environment by the combustion of non-renewables, we are also losing these non-renewable materials that could be useful in the future such as to create plastics. Because of these problems, these non-renewable energy production systems need to be phased out and therefore the renewable systems need to scale up so as to reduce the reliance on fossil fuels.

An issue with renewable energy production methods, such as solar and wind, is that they follow the weather and natural availability patterns, hence their production is independent from demand. There is therefore an overarching need to harmonise demand with production. There are also ways of storing bulk energy such as lithium ion or nickel metal hydride batteries that have a large specific energy [2], meaning that they can store a lot of energy per gram of material. However for many of these high specific energy storage methods there is a limit in power density, meaning a limit in how quickly this bulk of energy is drawn.

Peak production methods are the type of methods that can quickly supply a large amount of energy with little latency. These are primarily used to fill in the deficit peaks that the renewable bulk production cannot fill. The current main peak supply method utilised is the burning of natural gas to power turbines that produce electricity. Having an efficient way to store otherwise wasted renewable energy that can input and output a high power could potentially be used to fill these deficit peaks instead of the combustion of natural gas to fill the peak energy deficits. Capacitors are energy storage devices that have a very high power output and can supply a lot of energy very quickly. One downside to capacitors is that they have a very low specific energy meaning they cannot store large amounts of energy per gram compared to the batteries mentioned earlier in this section. An energy storage component that has performances somewhere between the batteries' high specific energy and the capacitor's high power density is an electrochemical ultracapacitor otherwise known as a supercapacitor. Supercapacitors use a capacitive electrochemical storage mechanism off of a surface reaction that gives both a higher energy density compared to a capacitor and a higher power density compared to a battery. For the use of grid scale energy storage, it has been theorised that one of the best options would be the deployment of a Hybrid Energy Storage System [3] that combines the high energy dense battery architypes as the main bulk energy storage solution with the high power dense supercapacitor that supplies the peak energy storage.

1.2 Enserv

The Enserv Group (Thailand/UK) is a major international company dedicated to development of new technologies for a sustainable future. Enerv has asked Swansea University to research scaled up manufacturing of supercapacitors. There are many veins in this collaboration ranging from the research of various materials to create each electrode from, to the creation of an asymmetric supercapacitor. This MSc project will focus on the development and optimisation of activated carbon inks for supercapacitor application, including early testing of Enserv proprietary activated carbon called "Enserv Super Carbon".

1.3 PROJECT AIM

The aim of this project is to explore the formulation of activated carbon inks for supercapacitor applications. The project was developed in partnership with industry (Enserv Group, Thailand/UK) targeting an AC anode ink for use as a high performing anode in an asymmetric supercapacitor [4], considering coating scalability matched with performance. This will be achieved through systematically testing multiple parameters to the ink and testing the effects of changing said parameters.

One main parameter that was used to optimise ink performance was testing what proportion of binder the ink will be made from. The project will focus on the use of ethyl cellulose as a binder expanding previous research for Enserv at Swansea University as an ideal candidate polymer for scale up aqueous supercapacitor applications, in view of it's compatibility with an aqueous electrolyte, compatibility with environmentally friendly and easily manageable and low cost solvent (e.g Diacetone Alcohol). All electrode inks that have been mixed in previous research for Enserv at Swansea University have used a 20% ethyl cellulose binder recipe, no binder optimisation process has previously taken place.

Literature Review [5] [6] in the sectors adopting different binder materials, other than Ethyl Cellulose, indicate that a 10-5% binder ratio are commonly adopted leading to an increase in the performance of the anode by offering more carbon material to store ions dissolved within the electrolyte. However, these papers all used different binders therefore using that amount a different binder, such as EC, may not perform in the same way. But one issue arising from decreasing the proportion of binder found in previous research is that the electrode material can flake off due to poor electrode-current collector adhesion or even cohesion within the electrode between two carbon particulates which will obviously decrease the performance of the electrode by removing a portion of the active material. Tests must be performed to find the optimum amount of binder that will give better performance but does not decohere from the current collector.

The combination explored in this project of ethyl cellulose as a binder and diacetone alcohol in activated carbon supercapacitor applications does not have a great deal of literature around it. Aside from the polymer, the key component in the activated carbon ink formulation is the activated carbon material itself. This project will focus on the use of Kuraray YP-80F activated carbon for testing polymer optimisation. This carbon was selected in view of availability, good performance demonstrated in previous research at Swansea University and

importantly extensive comparable literature, therefore this Kuraray YP-80F activated carbon is an optimum test bed and reference material. Enserv has also been developing a proprietary manufactured activated carbon (still limited availability at time of this project) called “Enserv Super Carbon”. Preliminary testing will be performed on this activated carbon, providing an early comparison of its performance to that of the Kuraray YP-80F.

Extensive electrochemical testing will be critical to the work presented. Each of the produced samples will be tested using a potentiostat to create cyclic voltammetry profiles, galvanostatic charge discharge peaks, electrochemical impedance spectroscopy and some multiple cycle tests to get an understanding of performance and durability of developed AC inks as anodes. A Scanning Electron Microscope will also be used to visualise the carbons used to create the electrode materials and to properly link the data from the potentiostat to what may be occurring in the electrode at a micro/nano scale. Before using the new type of carbon being tested in the anode it would be useful to properly characterise the Super Carbon so as to understand the comparison between the YP-80F carbon anode and the Super Carbon anode and know why they could be different.

CHAPTER 2: Literature Review

2.1. Supercapacitor principles

This section will report on the principles of supercapacitors including details such as the general principals of how they work and says why a more porous and higher surface area density material works best and suggests that activated carbon is a potentially good material for this use.

One of the main energy storage mechanisms of supercapacitors is through the formation of an electrical double layer [6]. An electrical double layer is formed when the charged ions are near the oppositely charged electrodes without undergoing a redox reaction. When this happens a large electric field is formed between them which supplies a potential difference on the electrodes. Over the years there have been multiple theories as to how the electrical double layer works. The first theory was the Helmholtz theory which proposed 1853 that there is a rather linear layer of electrons giving a linear potential field with the equation written below.

$$C_H = \varepsilon_0 \cdot \varepsilon_r \cdot \frac{S}{d}$$

Where C_H is the capacitance, ε_0 is the permittivity of free space, ε_r is the relative permittivity of the dielectric electrolyte, S is the surface area and d is the thickness of the double layer. The second theory created in 1910 was the Gouy-Chapman theory where it was noted that the ions in solution with opposite charge to the closest electrode migrate to get closer to the electrode. While doing so the concentration of the oppositely charged ions gets higher closer to the electrode causing an exponential decay of potential the farther away from the electrode the ions travel until the effect of the charged particles is negligible. The zone in which the concentration of ions building up influences the potential of the electrode is called the diffusive layer and any electrolyte that is not in the diffusive layer is called the bulk layer. The final theory and the model is the Stern model that combines the Helmholtz and the Gouy-Chapman models by still having a diffusive layer that induces an exponential decay in the potential field that decreases the further away from the electrode, but it also has the Stern layer and stern plane that is the separation of the very closest ions and electrode these three models are demonstrated in figure 2.1.

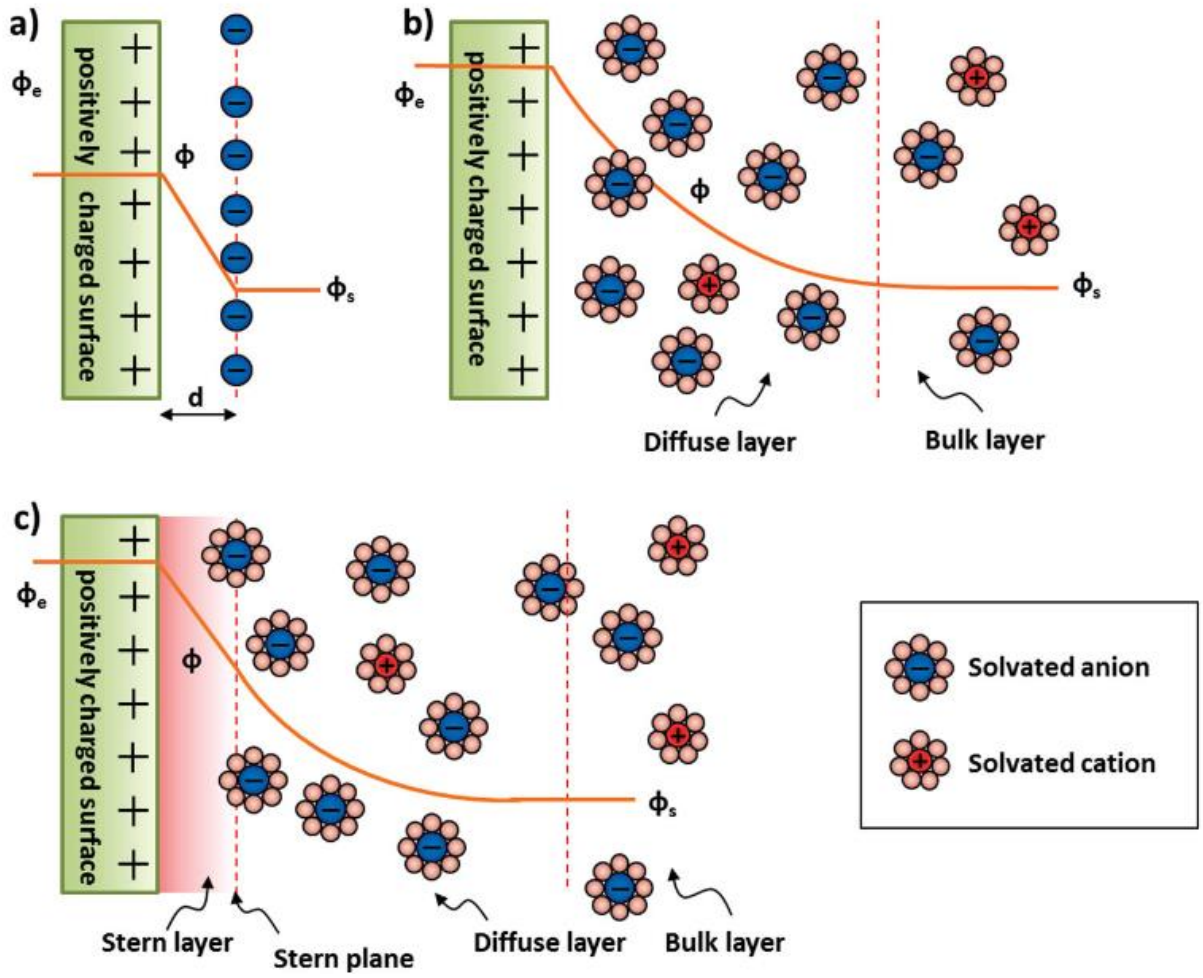

FIGURE 2.1:
Diagram to show the different theories for electrical double layers.
a) Helmholtz showing a linear trend between the charged surface and the ions b) Gouy-Chapman showing an exponential decay between the charged surface and the charged ions c) Stern model showing a linear model until the stern plane then it goes into a exponential decay [6]

To consider the optimum material for the electrode it is necessary to consider its requirements. Because only a certain number of ions can be stored per area/volume of electrode material, a material with a very high surface area to volume ratio would be the best material for the electrode to induce the strongest potential. Therefore, the ideal material for the electrode should be porous to increase the surface area to volume ratio and to have enough volume to store the charged ions. However, the electrode also needs to be conductive to allow the electron mobility and to allow the electrons move in and out on charge and discharge. To make the electrode an ink slurry must be made and printed/coated onto a current collector for the ink to stick to the current collector and not to flake apart a binder can be an ingredient in the ink. Too much binder can however decrease the capacity of the electrode and therefore should be minimised where possible.

The most commonly used electrode material for supercapacitor electrodes is activated carbon due to the very high specific surface area [6]. Activated carbon is a form of carbon that has been treated/activated either through high temperature or chemically, or both, to create very small nano pores throughout the structure which gives the material its high specific surface area. This surface area is ideal for a supercapacitor because it gives the material a hierarchical pore structure which has three main benefits. Firstly, the larger gaps or pores, larger than 50nm. allow the electrolyte to fully infiltrate the electrode, secondly the slightly smaller pores of between 2-50nm facilitate anode transport and finally the pores that are less than 2nm are pores that allow charge storage [6]. One issue with activated carbon ions that is they are not as conductive as many carbon materials therefore these electrodes often need to have a conductive material added to them to increase the conductivity and therefore increase the performance of the electrode. It has been theorised by Raymundo-Piñero et al [8] that the optimal pore size is around 0.7nm. in an aqueous electrolyte.

2.2. Previous Literature on Activated Carbon Electrodes

This section shows previous literature on how activated carbon electrodes have been made for supercapacitors in other studies and how an initial ink was created using a polymeric binder, a solvent, the active material itself and some form of conductive carbon to better the conductivity of the electrode, finally this section reports on the lack of literature around the use of an ethyl cellulose binder which is a great alternative for the other binders used in reported literature because ethyl cellulose is derived from a natural resource and is therefore sustainable, and it is also non toxic so is a better alternative for scaled up manufacturing because the low toxicity decreases the manufacturing cost as well as being a great match with diacetone alcohol which is a comparatively low toxicity solvent.

Demarconnay et el [5] created an activated supercapacitor using activated carbon. The ratio of components to the recipe of the ink is very important. In this research they used 80wt% activated carbon, 10wt% acetylene black (a sub type of carbon black) which is manufactured by the incomplete combustion of heavier petroleum. The carbon black's use in this case is to increase the conductivity of the electrode. The final 10wt% of the electrode is made from Polyvinylidene fluoride (PVDF) as a binder. Figure 2.2A shows the cyclic voltammogram profiles of the ac/ac supercapacitor. The vague principle of cyclic voltammetry is that the voltage is the independent variable that is changed at a set rate between two voltage limits and therefore the voltage is set as the x axis and the current is the dependant variable that is

measured and therefore is on the y axis. In this figure there are multiple CV curves that have changed the positive voltage limit as they were testing the stable voltage range of this electrode material. The galvanostatic charge discharge (GCD) curves are shown in figure 2.2b, GCD testing is the act of, starting at a set voltage limit, applying a set current and timing how long it takes to reach the other voltage limit then the current is reversed, and this is timed again. The standard way to graph this is to plot time on the x axis ad voltage on the y axis as shown in this figure. This figure also shows many GCD plots that once again change the upper voltage limit.

At lower voltages Figure 2.2A shows a relatively rectangular shape which is comparable to many capacitor voltammograms, however once the maximum cell voltage window is increased by roughly 1.1 volt the current increases significantly, this was explained in the paper by there being a redox reaction happening around this voltage. It is also visible that the final cycle that ends at 1.7V has less specific current than the previous cycle, this does not follow the usual trend that the maximum specific current goes up with voltage. This is also attributed to the phase change and gives a good indicator that the supercapacitor should not be discharged at more than 1.7V. The galvanostatic charge/discharge graph, Figure 2.2B again demonstrates a typical capacitor's window at lower voltages but once at higher voltages there is again some distortion which is also attributable to the same redox reactions that were happening in the cyclic voltammograms.

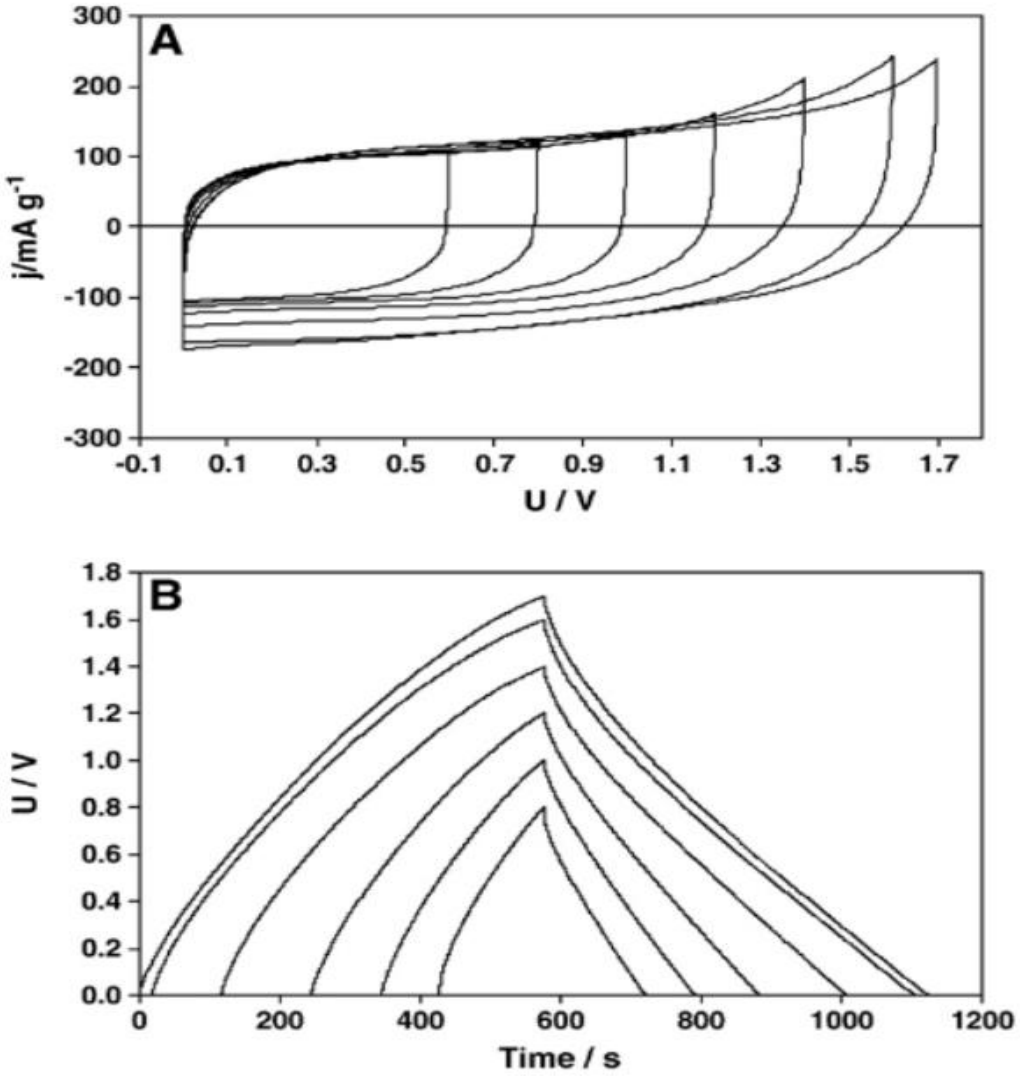

Figure 2.2:
An AC/AC supercapacitor in 0.5mol L^{-1} of Na_2SO_4 (A) Cyclic voltammograms ($2mVs^{-1}$) with differing voltage limits on each cycle and (B)galvanostatic ($200mA\ g^{-1}$) charge discharge showing multiple repeats at a differing upper voltage limit [5]

In many electrochemical energy storage devices, the existence of phase changes can be detrimental to the lifecycle of the device by removing the active material that can be used to store the energy. This paper compares the maximum discharge capacity per cycle for multiple voltages tested, this is shown in Figure 2.3. The main trend shown in Figure 2.3 is that as the voltage is increased, the maximum discharge capacities increase, with one main exception in 1.7V. All the supercapacitors at 1.6V or below has an initial period where they do not fit the trend but then they finally settle out on a shallow slowly decreasing line. The only line in this graph that is not in accordance with the trends is the line of the capacitor that was discharged at 1.7V, which again is attributed to the redox reaction somewhere in the capacitor that

decreases the amount of active material and therefore decreases the overall specific capacitance.

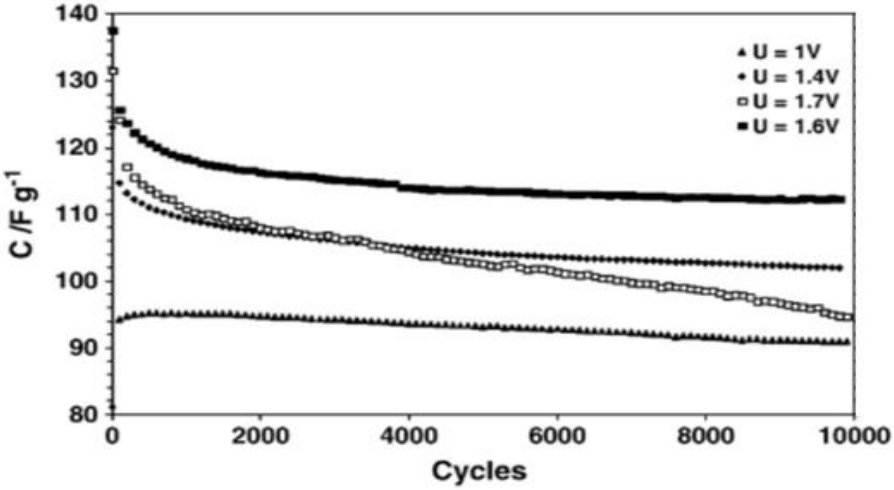

FIGURE 2.3:
Maximum specific discharge capacities per cycle of the AC/AC supercapacitor at varying voltages [7]- note the samples being stable until 10,000 cycles except from when it was tested at a too high voltage window

Demarconnay et el [5] showed that it is possible to have a better performing capacitor than that that uses only AC/AC symmetric supercapacitors, this limits the overall capacity density of the supercapacitor. It has been shown by Brousse et el [9] and others [6][10] that is possible to create an asymmetric supercapacitor that can supply around 2V. An asymmetric supercapacitor is a supercapacitor in which the two electrodes are not made from the same materials. The most common asymmetric supercapacitor is where the positive electrode, the cathode, is doped with a material with a higher capacitance, commonly manganese oxide (MnO_2) and the negative electrode, the anode, is an activated carbon electrode as used by Demarconnay et el [5]. The ink ingredients in the research by Brousse et el [9] used an ink that was 90% AC, 5% graphite for conduction instead of carbon black and 5% PTFE as a binder.

The cyclic voltammetry graph for this activated carbon anode is shown in Figure 2.4b, it shows a curve that is not as rectangular and differs significantly from that produced by the research done by Demarconnay et el [5]. There is a big spike in the negative region at -1.3V, this can be attributed to the Hydrogen Evolution Reaction (HER), which is when the water in the electrolyte undergoes electrolysis and produces hydrogen. The HER reaction means that it would not be safe to operate a supercapacitor with the anode voltage any lower than -1.3 volts as it may harm the life of the supercapacitor if the electrolyte is aqueous. This research found that the lifetime of the 2V supercapacitor was similar to the stable supercapacitors at voltages below 1.6V as shown in Figure 2.5, the columbic efficiency per cycle. The coulombic efficiency is the ratio of how much energy was retained from at the start and at the end of the charge cycle. The fact that the coulombic efficiency remains near 100% means that the supercapacitor is stable even at 10,000 cycles.

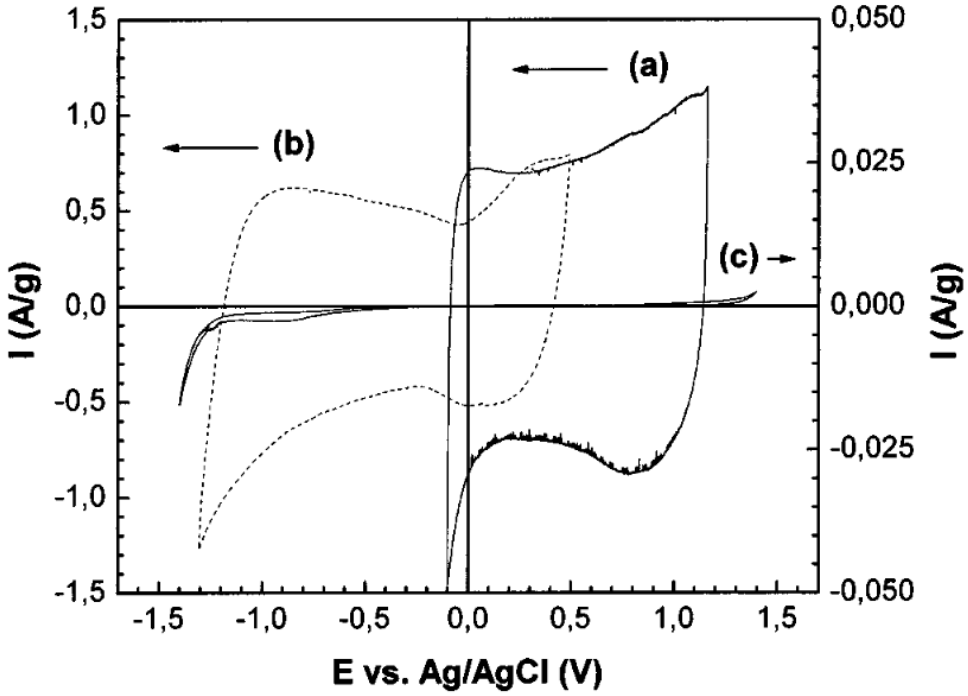

FIGURE 2.4:
Cyclic voltammetry of a) composite MnO_2 electrode, b) composite AC Electrode (90wt% AC) and d) titanium grid current collector. Scan rate 5mV/s, electrolyte 0.65M K_2SO_4 [8] – note the big spikes at the negative voltage limit that occurred because of a hydrogen evolution reaction

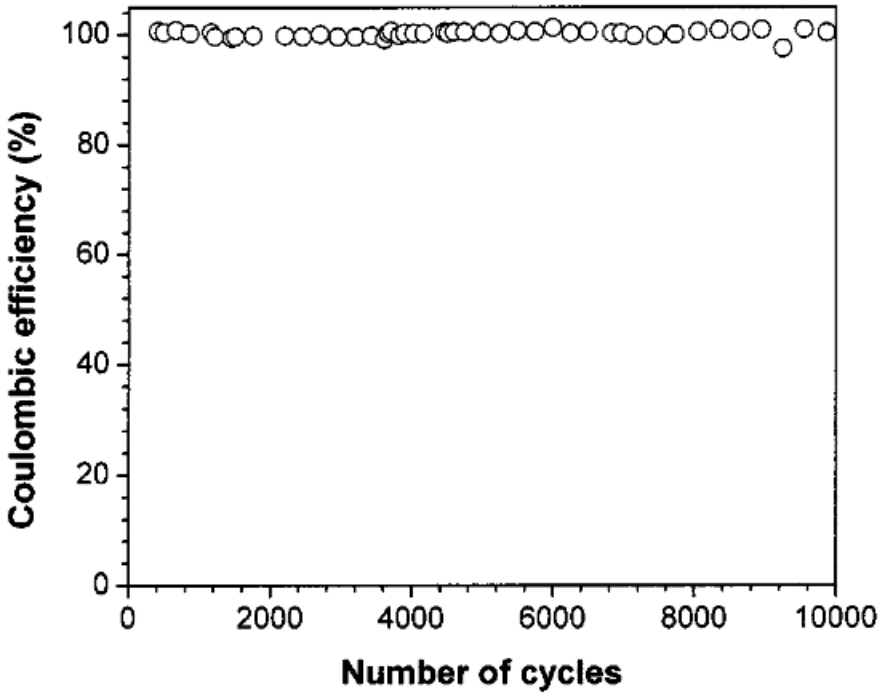

FIGURE 2.5:
Columbic efficiency of the capacitor cycled at 2.2V that is stable for 10000 cycles [4]

Other research on activated carbon electrodes for supercapacitors focuses on the carbon material itself. One study on this area was performed by Gamby et al [11] this research tested multiple different carbons form the PICA company by originally characterising the surface area of the carbons by Brunauer-Emmett-Teller (BET) testing. These carbons were then tested using a 95% activated carbon and the other 5% PTFE electrode. These electrodes were electrochemically tested to get a specific capacitance using a GCD test at 10mA/g the graph of the BET specific surface area vs the specific capacitance is shown in figure 2.6. It shows experimentally that the general trend is that as you increase the carbon's surface area the capacitance increases. This is not always the case, for example the highest capacitance datapoint on this graph is not the carbon with the highest BET surface area, the data point for PICACTIF SC carbon which was a certain type of carbon that was tested. This was later shown via EIS that this increased capacitance was formed from a large mesoporous volume that allows accessibility for the ions to absorb on the surface.

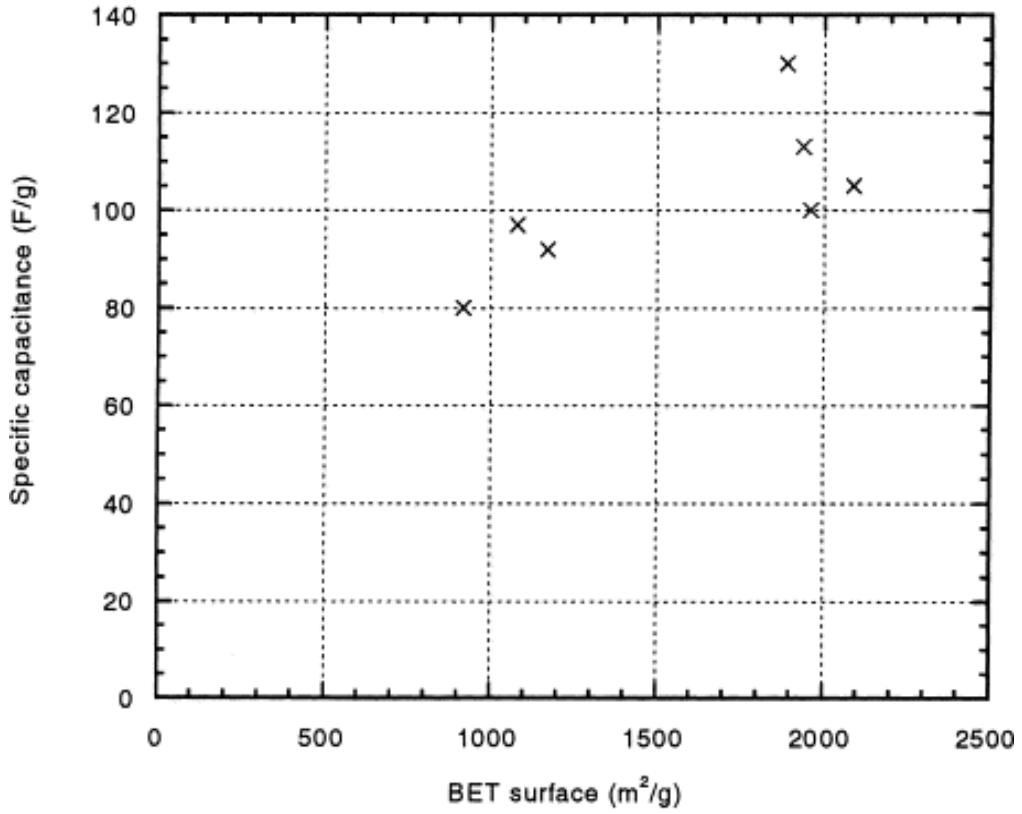

FIGURE 2.6:
Specific capacitance Vs BET specific surface area that displays a general trend of as the surface area increases the general capacitance of the electrode increases [11]

The Binders used in reviewed literature are either non renewable or are toxic or both. This makes the environmental and economic effect of manufacturing these electrodes high. One potential material, Ethyl cellulose (EC) is a great alternative material for the binder because it is derived from cellulose aa very readily available sustainable resource, and it has a very low toxicity which reduces any processing costs of making the electrodes. As well as the actual material itself, EC has shown in previous work with Enserv at Swansea University to work well in partnership with diacetone alcohol as a solvent which again is useful due to its relatively low toxicity, especially compared to other solvents used in reviewed research. Unfortunately, EC is not as prevalent in literature and there is very little research performed using ethyl cellulose as a binder for supercapacitors, this work also tests the use of ethyl cellulose as a binder and diacetone alcohol as a solvent and compares it to the previous literature using different binders and solvents. What literature there is on ethyl cellulose does demonstrate that it does work as a binder but is often used in ranges outside of the scope of thesis project, for example coating activated carbon on indium-tin-oxide to create transparent energy storage devices [12] or to coat electrode materials using electrophoretic deposition [13].

CHAPTER 3: Materials and Methodology

3.1 Materials

Activated carbon ink was composed by 4 main components: activated carbon, binder, carbon black, and solvent:

- Activated carbon: for the optimisation study of the ink, the project focuses on the use of Kuraray YP-80F (Kuraray, Japan). From datasheet provided by Kuraray, this AC supposedly has a BET surface area of 2,271 m^2/g
  In later chapters, a carbon created by Enserv Power is analysed and tested to compare it to the industrially available Kuraray YP-80F
- Binder: as mentioned Ethyl Cellulose (from Aldrich Chemistry, 200697-500G) was adopted as binder; understanding its effect on electrochemical performance at different concentration isa key point to the work performed
- Carbon black: small amounts of carbon black are typically has the role to increase electrical conductivity of the deposited layers; Carbon Black (Super P) was adopted at affix concentration of with a 7:1 ratio of activated carbon to Super P.
- Solvent: Diacetone Alcohol was adopted, based on preliminary work performed by Swansea University with Enserv. Diacetone alcohol is an alcohol with a relatively low toxicity with a boiling point of $166^{O}C$

More details on materials adopted are presented in next sections, while discussing their processing.

3.2 Activated Carbon Ink- Material constituents, formulation and coating

This section explains the preparation of the activated carbon inks, from description of its constituents, the presentation of mixing process, to the description of deposition through bar coating over selected substrate

The ink was made from the activated carbon active material, the main carbon used was Kuraray YP-80F as it is a widely industrial available carbon to build the original ink recipe with. YP-80F is an activated carbon made by Kuraray specifically for EDLC applications in the datasheet provided by the supplier Kuraray YP-80F is supposed to have a specific surface area of 2271 m^2/g and an initial weight capacitance of 31.7 F/g at room temperature. It aims to have grain sizes in the order of single number of microns and has a target BET specific surface

area of 2271 m^2/g [14]. This material has already been shown to perform well as a EDLC supercapacitor in previous research where it has gotten around 94-82 F/g [15] using an electrode composed of 85 wt% activated carbon, 8 wt% Super C45 conductive carbon and polytetrafluoroethylene (PTFE) using a PC + TEABF4 electrolyte so is not comparable to the results shown in this thesis, which is a binder that is being avoided in this study due to toxicity, and isopropyl alcohol as a solvent. Because this material has shown good performance before, it was decided to use as a starting testing material to base the ink recipe around, other carbons can be substituted into these recipes to determine how they perform in the same situation.

A solvent is needed for dispersing the components of the ink ingredients whilst having a low volatility which helps with the film integrity during the drying process. The chosen solvent was diacetone alcohol (DAA) as it has a relatively low toxicity and is relatively safe to work with therefore is easily scalable. Ethyl cellulose (EC) was used as the binder as it has worked well with DAA on previous projects. EC is a polymer that has been derived from cellulose, a commonly found material in plants, but some of the hydroxyl groups within the glucose molecules in the cellulose are converted into ethyl groups so this material is easy to source/produce and has no toxicity/ prediction issues. A conductive Super P carbon black was added to aid the conductivity of the electrode to enhance performance.

To make the inks, the EC was dissolved in a wt 1:9 ratio of EC to DAA by heating it to around 50 ^{O}C with magnetic stirring for an hour. Each ingredient was weighed out in the correct proportions such that there was the correct amount of dry ingredients (not DAA) to make 2 g of dry material. These ingredients were then put into a FRITSCH ball mill Pulverisette 23 shown in figure 3.1. The slurry is then mixed primarily mixed at 15 Hz for a minute to ensure the ball mill is seated properly, it was then staged up to 30 Hz for another minute then finally mixed at 50 Hz for 5 minutes. After this more DAA was added and mixed until the ink was the correct rheology for bar coating, at this point the ink was mixed at 50 Hz for another 10 minutes to ensure homogeneity.

FIGURE 3.1:
Image of the FRITCH Ball Mill Pulverisette 23 used to mix the ink until the correct viscosity

During the mixing the pre-cut 2x10 cm substrates were prepared by roughing up 2 cm^2 of one end of the sample, where the electrode material was to be printed, with sandpaper if this is possible (depending on the test substrate material). It was then washed using IPA and Methanol, left for a minute to dry and then weighed. The substrate was then clamped into the bar coater K Control Bar Coater shown in figure 3.2, cleaned again using IPA (Isopropyl alcohol) and left to dry for 30 seconds. The ink was then deposited onto the end of the substrate that has been roughened using sandpaper and bar coated with an aim wet thickness of 24 μm and left in an oven overnight at 120 ^{O}C then weighed the next day to find the dry coating mass. The coating of the electrode material was done as soon as possible after the ink was made to prevent the solvent in the ink evaporating and drying up the ink. The bare substrate that would be submerged in the electrolyte during testing was then coated with epoxy resin by hand and set under a 302 nm wavelength UV light for 10 minutes per side. The finished electrode is shown in figure 3.3.

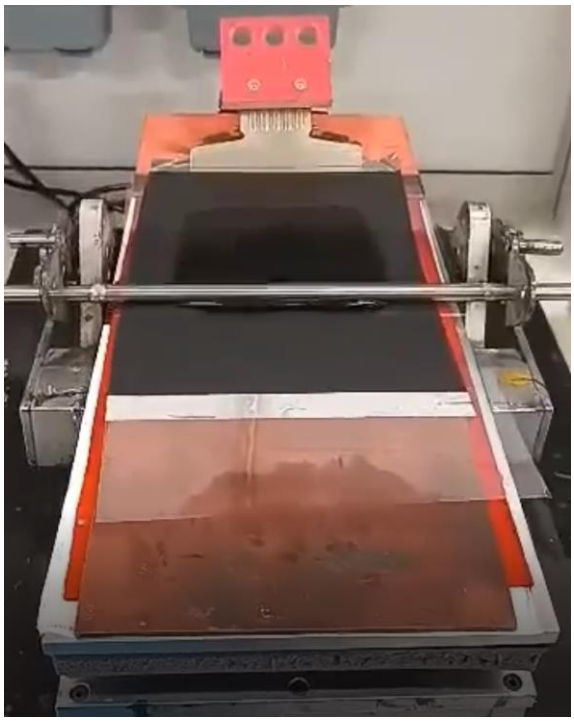

FIGURE 3.2:
Image the K control bar coater coating a larger surface area activated carbon ink onto carbon coated aluminium

FIGURE 3.3:
Image epoxy covered 10% EC electrode on nickel that has been covered in epoxy glue to prevent the nickel from having any effects on the electrochemical testing

3.3. Activated Carbon Powder Characterization

This section describes the material characterisation performed over the activated carbon powder. Activated carbon is at the core of supercapacitor performance, hence it was critical to verify the AC adopted, in case of the Kuraray YP-80F to verify that conform with datasheet (see results) Scanning electron microscopy (SEM) was used to image the carbon particles as to look at the particle sizing and to gauge the shapes and texture of the particles.

Activated carbon was also analysed through the Malvern Morphologi 4 this is an instrument created by Malvern Analytical which can both analyse the particle sizes of the individual carbons and perform Raman spectroscopy of the carbon powders this equipment is shown in figure 3.4. This equipment allows the automatic optical imaging and size analysis of particles, while being integrated with RAMAN spectroscopy. Characterisation of AC powder was performed over 1000 particles per carbon tested and the same machine was used to create Raman spectrograms of the carbon.

FIGURE 3.4:

Image of the Malvern Morphologi 4 Raman and particle size analysis equipment

Raman spectroscopy uses the inelastic scattering of photons from a laser on the surface of the tested material. This reflected Raman scattering provides information about the vibrational modes in the system and therefore can detect certain bonds within the carbon being tested. The carbon was loaded in a stainless steel well as pictured in figure 3.5, but not compacted so that the surface of the carbon particles was not affected. The prototype Morphologi 4 uses a green Raman laser specifically designed to measure carbons. However, the measurement of such small particles even with high power is challenging, so each particle was also measured (ten in total) at a low laser power (2 mW) for 1200 s (20 mins). As well as just the carbon, the carbon coatings were imaged using Alicona 3D optical microscope shown in figure 3.6 to inspect the surface finish from the bar coating and ascertain how the coating had dried. The Alicona 3D microscope can create a computational model the surface of the electrodes by collecting images at various focal points and stitching the most focused parts together at different heights on the model to create the overall surface

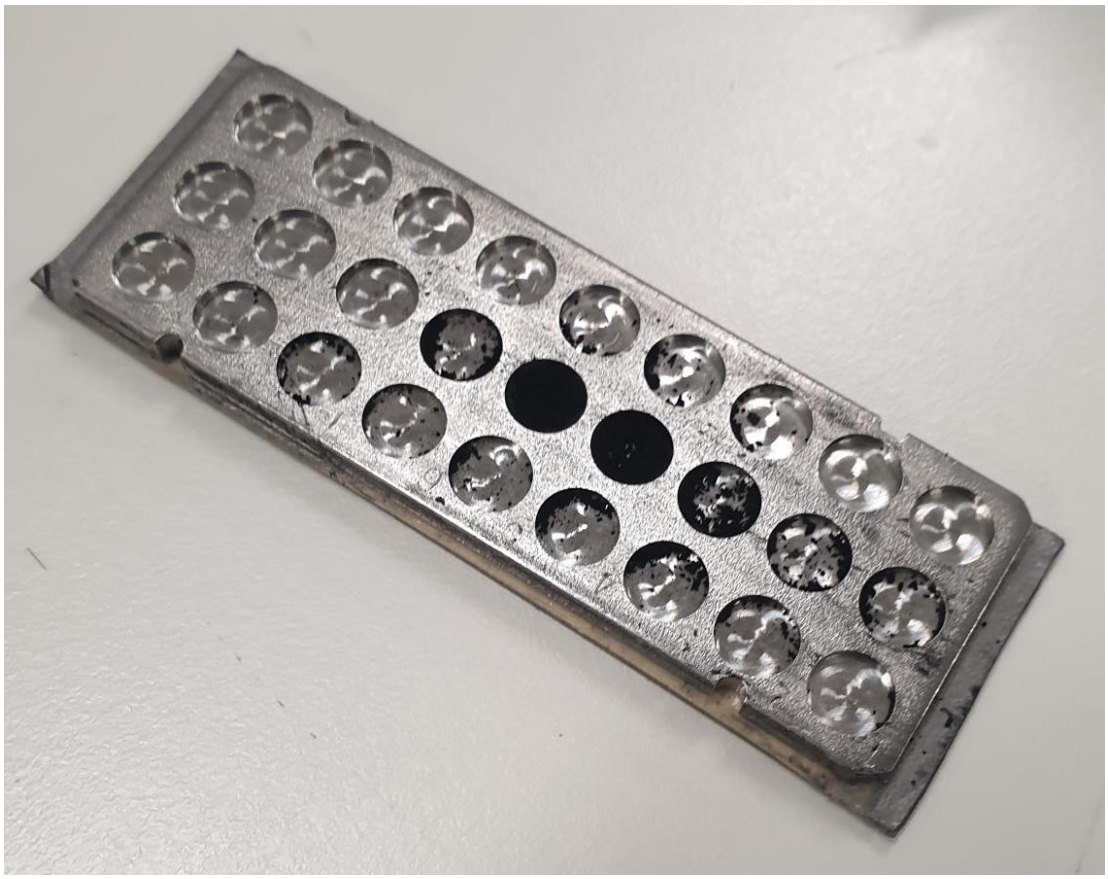

FIGURE 3.5:

Image of the carbon Raman testing setup

FIGURE 3.6:
Image of the Alicaona 3D light microscope

3.3 Electrolyte Preparation and Electrochemical Testing

This section explains how the general electrode material was electrochemically tested to demonstrate how well each ink recipe performed as a supercapacitor. It explains the three-electrode testing setup to test the electrodes by the three main electrochemical testing methods which are; Cyclic voltammetry (CV), galvanostatic charge discharge (GCD) and electrochemical impedance spectroscopy (EIS), and how they are tested and suggests methods in which performance is measured using the results of these tests.

Before testing the electrodes, the electrolyte was made by mixing up 200ml of 0.5M aqueous sodium sulphate solution and bubbling nitrogen through it using a mass flow controller for an hour immediately before testing. All electrochemical tests were performed using a 3-electrode setup, as shown in figure 3.6 on a biologic potentiostat. The three electrodes that were used were firstly an active working electrode which is the electrode that has been synthesised and is being analysed, secondly a silver/silver chloride reference

electrode that has known electronegativity and can therefore set a correct zero point, and finally a platinum counter electrode that performs the opposite electrochemical reactions to those performed by the working electrode.

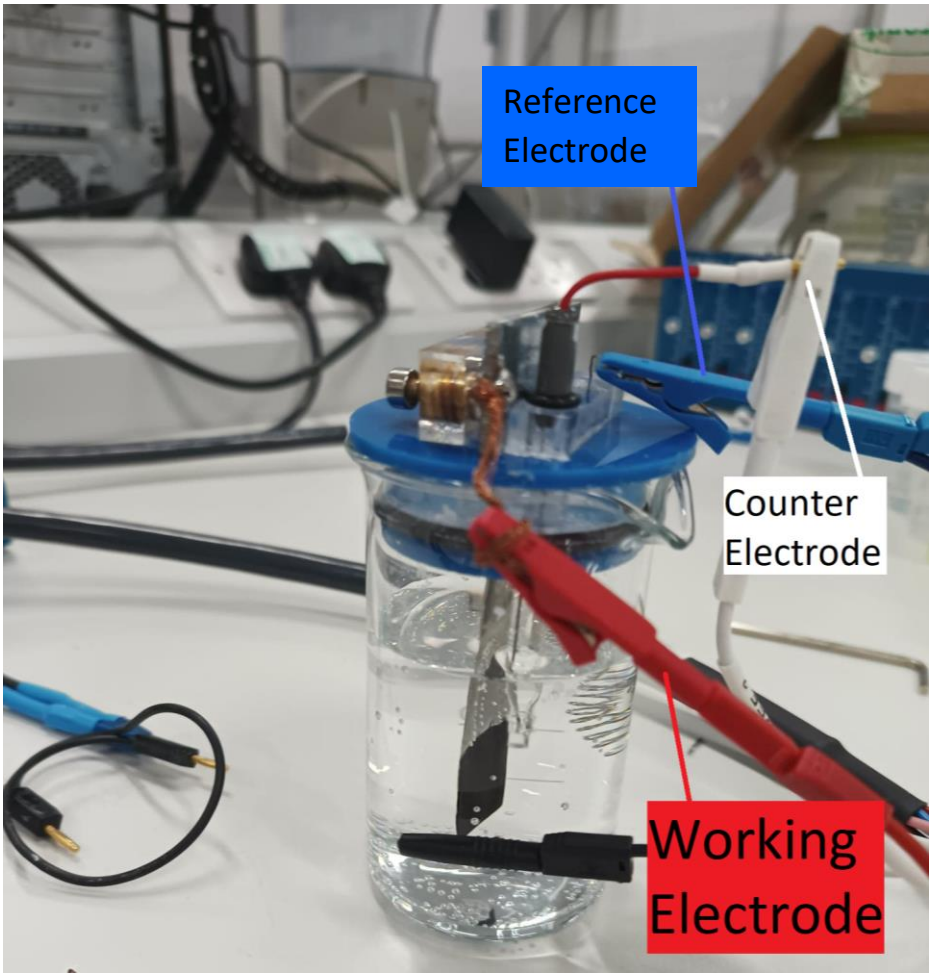

FIGURE 3.6:
Image of a three-electrode setup labelling the reference electrode being the blue clip attached to a platinum electrode visible in the right of the testing beaker, counter electrode in the red clip that leads to the silver/silver chloride electrode, and the working electrode in red attached to the Nickle substrate with a carbon electrode coating on the submerged end.

3.4 Cyclic Voltammetry Testing

CV is tested by starting at the open circuit voltage then applying changing the voltage and measuring the current produced, the voltage applied is applied in a set rate then once the voltage hits the pre-determined voltage window edge, the polarity of the input voltage rate is reversed and runs until the voltage hits the opposite limit. This waveform can be shown in figure 3.7. Segment 1 is an applied voltage between the open circuit voltage to the upper voltage limit, segment 2 shows when the voltage rate's current is reversed and goes towards the bottom voltage limit, segment 3 goes back up to the upper voltage limit. This was repeated 5 times to check for reliability. During this waveform cycling the current produced is recorded and plotted against current to give a CV curve as shown in figures 2.2 and 2.4. The first thing to look at with CV is the shape of the curve. An ideal capacitor will produce a fully rectangular CV curve; therefore, the CV curve of the tested electrodes should be as rectangular as possible but will never be fully rectangular so it will have a shape similar to that in figure 2.2a. Cyclic voltammetry is also used to determine whether the electrode is stable in the testing electrolyte, if there are any redox reactions occurring during testing there will be evident redox peaks in the CV curve. It is useful to see if there are any redox reactions happening because these could be irreversible phase changes that can permanently damage the electrode and therefore reduce the cycling capability of the electrode. Another test that CV can be useful for is determining the limitations of the electrolyte. If the potential goes to high or low in an aqueous electrolyte,

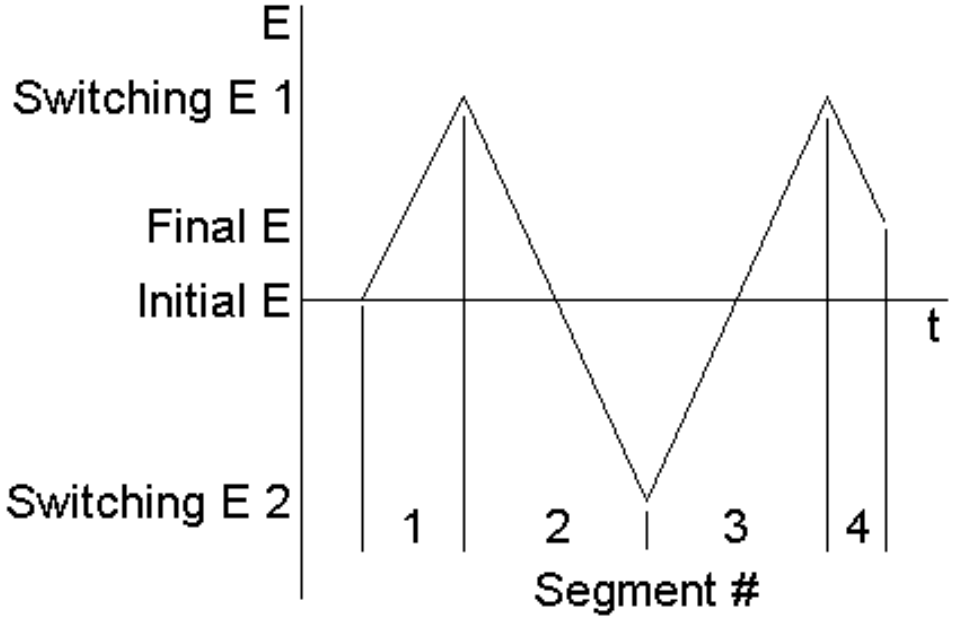

FIGURE 3.7:
Voltage waveform of a typical CV test [16]

it can either cause oxygen or hydrogen to de-bond from the water and form O_2 or H_2 gas. The oxygen evolution reaction (OER) happens when the potential goes too high (around 1.2V compared to silver/silver chloride [17]) and the hydrogen evolution reaction (HER) happens when the potential goes too low (below 1V). The final main use of CV testing is that the specific capacitance can be obtained using the area/integral of the CV curve by using the formula.

$$C = \frac{\int (I)\, dV}{2 \times (^{V}/_{S}) \times \Delta V \times m}$$

Where C is the specific capacitance, I is the current, V is the voltage, V/s is the scan rate and m is the mass of active material coated onto the electrode that can be worked out using the mass of coated material and the ratio of dry active material, this value is used instead of the weight of electrode material after curing as it is convention to use the mass of active material so they capacitances can be easily compared even when the proportions of ingredients in the electrodes are different. Finally ΔV is the voltage window. In these tests, the electrodes were tested at 2 different voltage windows, firstly the wider range of -1V to 0.6V, this test determines how the material and electrolyte performs across the full stable voltage and if the higher/lower voltage has any effect on the hydrogen or oxygen evolutions of the electrolyte. The second voltage window that was performed was the window between -0.5V and 0.5V that purely determines the performance of the material, this gives a good indication of how the carbon electrode would perform in other more stable electrolytes. Multiple voltage scanning rates were also tested for each electrode, these scanning rates were 10mV/s, 20mV/s, 25mV/s, 30mV/s, 40mV/s, 50mV/s and 100mV/s. Multiple scanning rates were used to determine how the material would perform at higher current densities as when the voltage is applied more quickly there is more charge per second going through the electrode and therefore a high current density arises.

3.5 Galvanostatic Charge Discharge testing

GCD is a method whereby a constant current is applied until a set voltage is reached, then once it has reached that voltage the electrode is discharged with the same current and the time taken to do this is recorded. For each test 5 GCD tests were performed to demonstrate reliability. For each electrode multiple currents were tested, these currents were again 10mA/s, 20 mA/s, 25 mA/s, 30 mA/s, 40 mA/s, 50m A/s and 100 mA/s. GCD testing is used to determine many factors. One main factor that it can analyse is the internal resistance of the electrode. As the electrode starts discharging it immediately drops some voltage and this

produces a vertical line, the internal resistance can be calculated by dividing the change in voltage of this line by the current scan rate. Another feature the GCD curves can determine is the coulombic efficiency, which is the percentage difference in the energy going in compared to the battery coming out, this can be determined using a GCD graph by using the ratio of time it takes for the electrode to discharge compared to the time it takes for the cell to charge when the charging and discharging current densities are the same, The coulombic efficiency is calculated using the ratio of charge throughput through discharging and charging this charge is calculated using the equation below.

$$Q = \sum \left| I + \frac{\Delta I}{2} \right| \Delta t$$

With Q being charge throughput (C), I being current (A), ΔI being the difference between charges between datapoints (A) and Δt being the difference in time between datapoints (s). using the two charge throughputs of both charge and discharge it is possible to calculate the coulombic efficiency using the equation below.

$$\eta = \frac{Q_{dis}}{Q_{ch}} \times 100\%$$

With η being the coulombic efficiency (%), Q_{dis} and Q_{ch} are the charge throughputs during both discharge and charge respectively (C).

The same two voltage ranges of -1V to 0.6V and -0.5V to 0.5V were tested, again to test the both the performance of the electrode material and how it works with the electrolyte and to just test the performance of the material by itself. To gain an understanding of how the electrode changes from one charge and discharge to the next, five GCD tests were performed each time the tests were taken.

3.6 Electrochemical Impedance Spectroscopy

EIS is measured by applying an AC voltage with varying frequencies and measuring how much of a phase shift occurs at these frequencies. At each frequency the impedance can be calculated. The EIS results are plotted by graphing up the imaginary component of the impedance with the real impedance in what is called a Nyquist plot. There is much to learn from the EIS Nyquist Plot, the first is the equivalent series resistance (ESR) that is the value of the real impedance at the point the plot starts (at the highest frequency recording), a high ESR can limit the performance of the cell because it is the overall resistance of the electrode. The presence of a semicircle on the Nyquist plot is often due to the presence of interfacial resistance between the current collector and the active electrode material. It is also possible to tell whether

the semicircle's resistance is correlated with charge transfer by resting at various potentials and seeing whether that effects the semicircle or just the tail that will change at lower frequencies.

When the electrodes were tested, they were tested using CV, GCD then EIS, then left to cycle for 2000 cycles and then the same tests were repeated after cycling. Unless stated otherwise, all figures shown are the results produced from the testing after cycling. Each electrode was also made and electrochemically treated three times using different batches of inks so as to detect anomalous results and to ensure reliability in data and ensure reliability in the formulation/coating/processing methods.

3.7 Substrate Selection: Carbon Coated aluminium Vs Nickel

An early challenge in the project was the identification of a suitable substrate onto bar-coat the activated carbon ink for testing. Two potential substrates were identified Nickel, a common substrate adopted in lab scale electrochemical testing of aqueous supercapacitors and batteries, and a carbon coated aluminium foil created by Cambridge Energy Solutions, a more affordable solution. In line with the scope of the project, aiming to replicate industrial scale conditions, the first early tests concentrated on the uses of carbon coated aluminium as an affordable flexible material that can aid with later on scale up with roll-to-roll printing. These early tests demonstrated significant issues with the substrate selection; In this section results of both a 20% EC, 70% Kuraray YP-80F Activated carbon and 10% Super P conductive carbon ink recipe and a 10% EC, 78.75% Kuraray YP-80F and 11.25% Super P conductive carbon ink recipe are reported, and they demonstrate how the carbon coted aluminium is not a suitable substrate

Figure 3.8 shows the CV curve of the 20% EC ink coated onto the carbon coated aluminium. An idea CV curve for a supercapacitor should be a rectangular shape, here the curve does not show the typical supercapacitor CV curve shape. This underlines a potential to have a huge internal resistance which lead to an overall capacitance calculated form this of only 0.20 F/g, which is a very poor specific capacitance and not representative of the materials used seeing as previous research at Swansea university had gotten around 20 F/g.

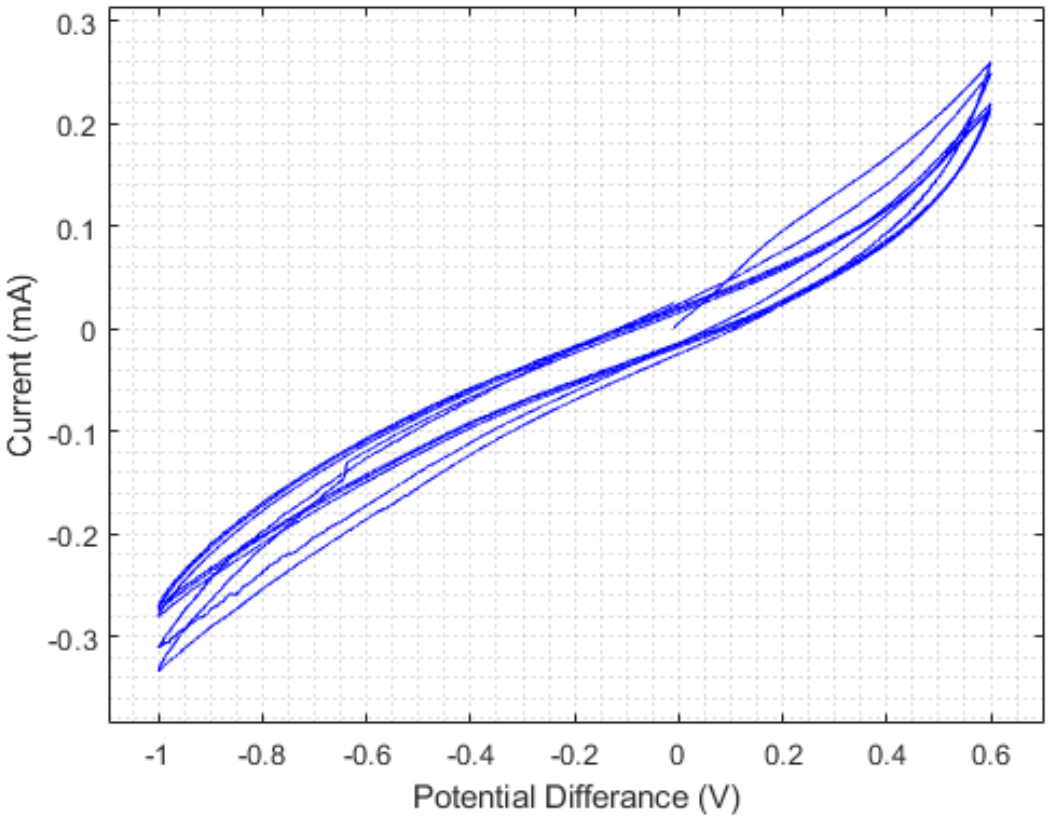

FIGURE 3.8:
CV curve of the 20% EC electrode using Kuraray YP-80F printed on a carbon coated aluminium at a scan rate of 10mV/s

The CV curve for the 10% EC Kuraray YP-80F ink on the carbon coated aluminium substrate is shown in figure 3.9. It can be seen that the shape of this CV curve is considerably better than the 20% EC on carbon coated aluminium. The rectangular shape can vaguely be seen in the positive end of the curve but trails off a bit in the negative region. The area of this curve is bigger than the curve produced by the 20%ink, and the currents achieved are an order of magnitude greater than the 20% Ethyl Cellulose test to the point where the specific capacitance is around 3.8 F/g when testing at 10 mV/s, which is still uncharacteristically low.

Figure 3.10 shows the GCD curve of this 10% EC electrode printed on carbon coated aluminium. The first point to note is the jump in voltage after the electrode begins to discharge. Using the 1ma current rate and the 0.26 V jump it can be calculated that the internal resistance of this electrode is around 26 Ω which is a very high resistance.

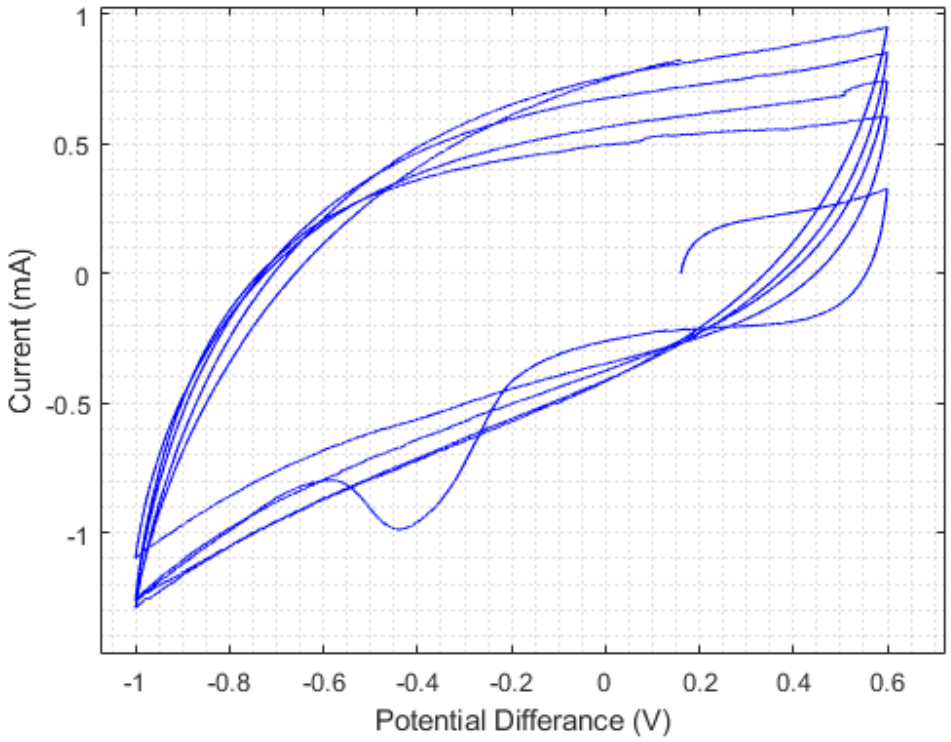

FIGURE 3.9:
CV curve of the 10% EC electrode using Kuraray YP-80F printed on a carbon coated aluminium at a scan rate of 10 mV/s

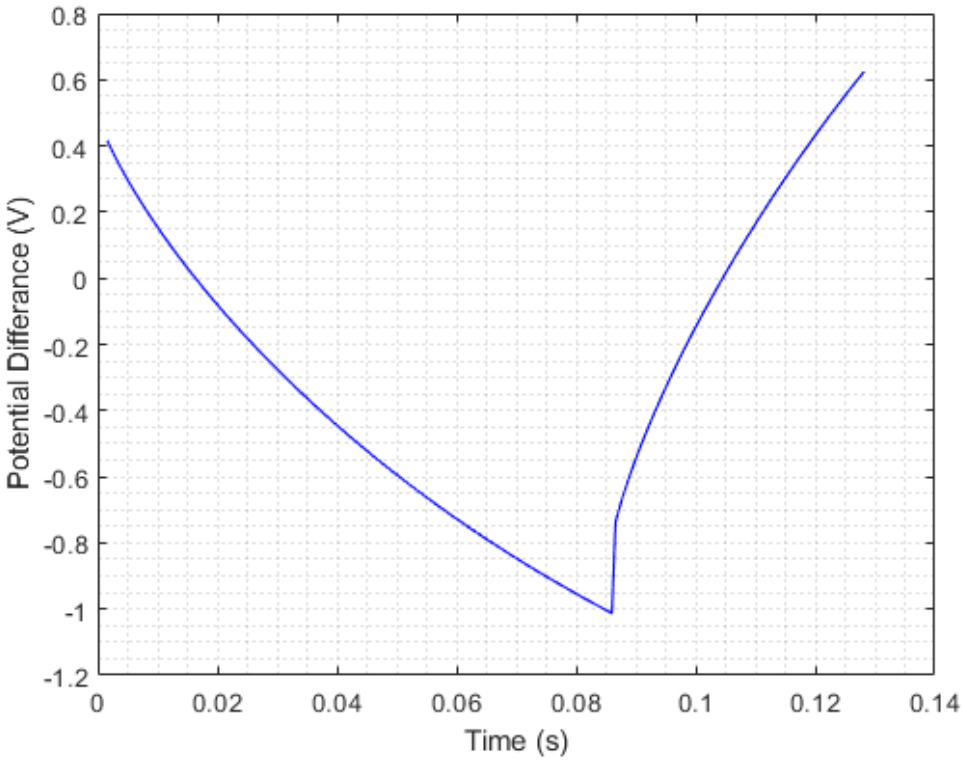

FIGURE 3.10:
GCD plot of the 10% EC electrode using Kuraray YP-80F printed on a carbon coated aluminium at a scan rate of 1 mA/s

The EIS graph for this 10% EC electrode is shown in figure 3.11. Of particular note is that the x intercept, the ESR, is 77 Ω, which again is still a high ESR for a supercapacitor electrode. The second point of note is the presence of the semicircle that shows that some resistance came from the interfacial resistance between the two carbon coatings.

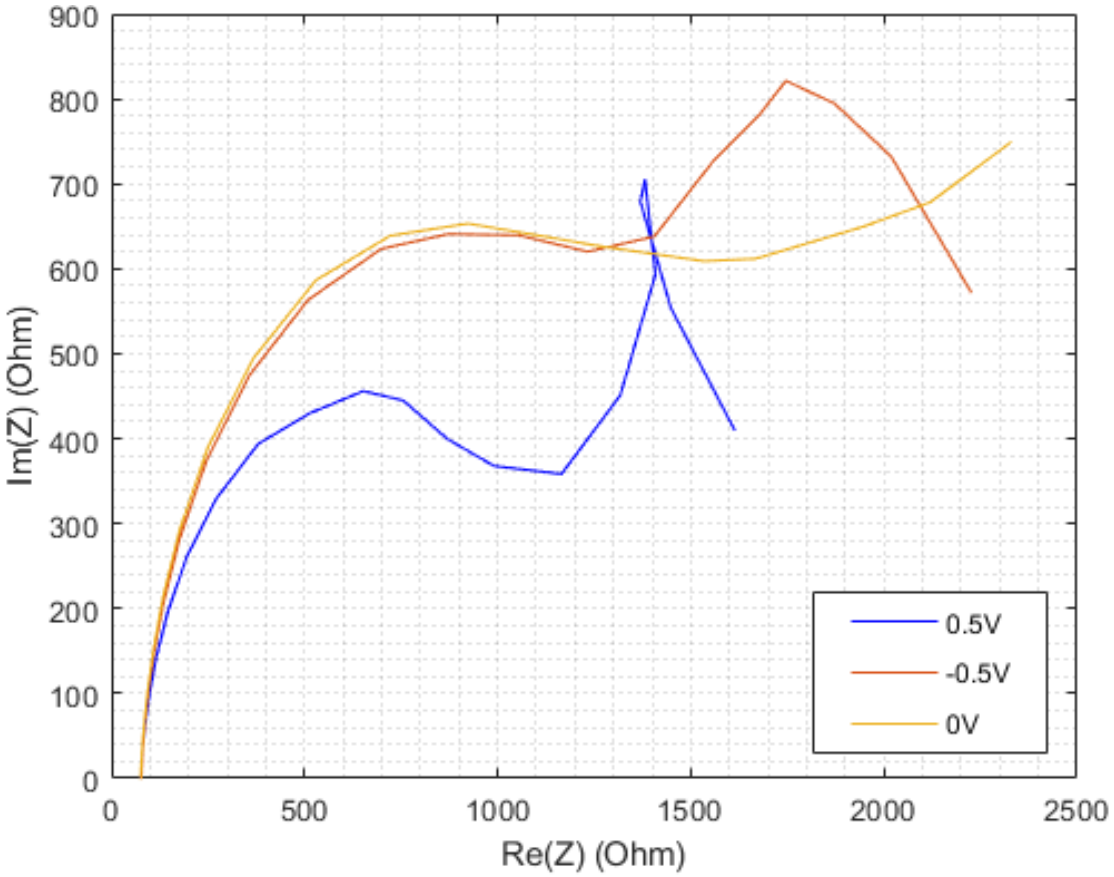

FIGURE 3.11:
EIS plot of the 10% EC electrode using Kuraray YP-80F printed on a carbon coated aluminium

It was originally hypothesised that the resistance in this electrode had mainly originated from where the current collector on the potentiostat attached to the carbon coating on the substrate. A quick surface resistivity test was performed using an ohm meter, the bare aluminium had a surface resistance less than 0.5 Ω compared to that of the carbon coating's 25 Ω. New electrodes were made where the opposite end of the electrode was bare uncoated aluminium so that it could make good contact with the metal plate attached to the potentiostat from which the current is collected.

Figure 3.12 shows the CV curve with the 10 % EC ink on the carbon coated aluminium with bare aluminium current collector. Compared to the 10 % EC ink on the plain carbon coated aluminium without the bare aluminium on the current collector in figure 3.8, this electrode is performing a lot better, it has slightly more of the rectangular shape, still uncharacteristically low currents.

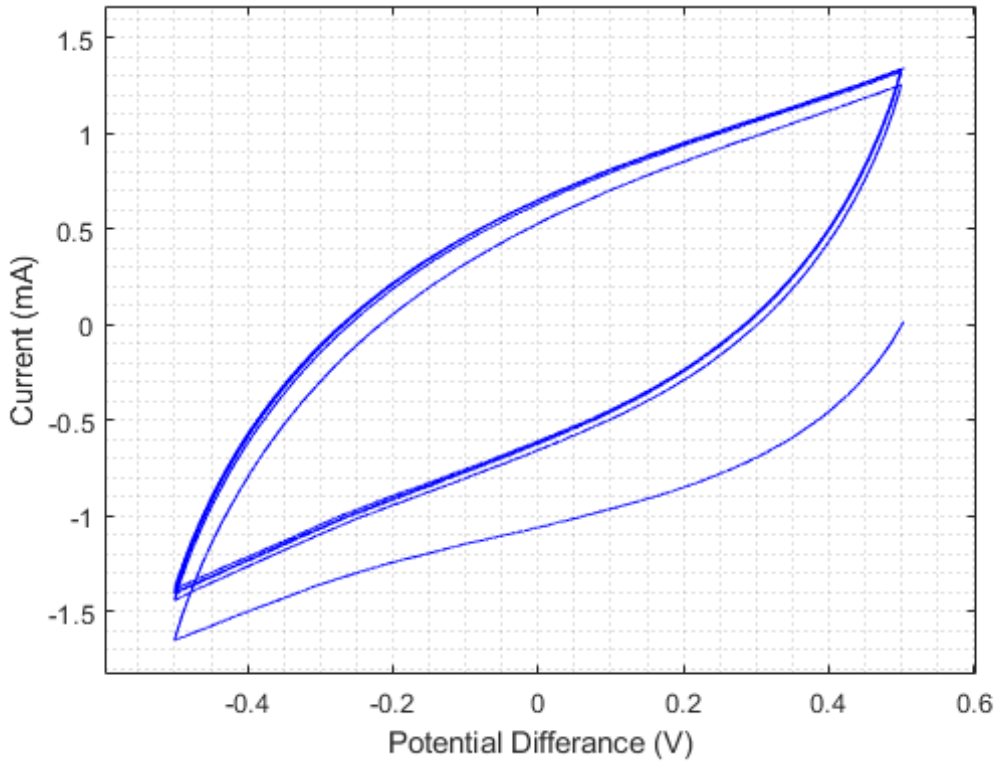

FIGURE 3.12:
CV curve of the 10 % EC electrode using Kuraray YP-80F printed on a carbon coated aluminium using bare carbon at the current collector at a scan rate of 10 mV/s

It was noted in one of the subsequent repeats of these experiments that where the epoxy hadn't been applied high enough on the substrate meaning that there was some bare substrate material submerged in the electrolyte and the bare substrate was sitting in the sodium sulphate solution electrolyte, the pre-applied carbon coating had delaminated from the aluminium as shown in figure 3.13. This could have been a reason for the high resistance in the electrode. These results were still significantly adrift from expectations by reference to other group research and so the decision was made to change the substrate back to a nickel substrate and to try and replicate previous prints using the 20 % EC ink and to test a range of inks with decreased binder content at both a 10 % and 5 % EC.

FIGURE 3.13:
Image of a 10% EC electrode using Kuraray YP-80F printed on a carbon coated aluminium with bare aluminium at current collector: notice the stripping of underneath carbon coating, demonstrating how the electrolyte damages the commercial carbon coated aluminium, making it a not adequate choice of substrate

The original testing was originally meant to determine how much changing the amount of binder in an ink recipe would increase the performance of an electrode by decreasing the binder quantity from 20% to 10% that was used in previous projects. The theory was that as the binder quantity decreases the more of the electrode is active material that is used for

functionality. Another benefit to reducing the binder content is to reduce the amount of polymer blocking the pores in the structure of the activated carbon to allow a greater degree of electrolyte infiltration and allow more ion storage and therefore increase functionality, however, through that experiment it was found that the use of the carbon coated aluminium had a large negative affect on the performance of the electrode. As stated previously, it was originally hypothesised that there was a large surface resistance between the carbon coating and the metal current collecting plate attaching the electrode to the potentiostat. The shapes of both figures 3.9 and 3.12 shows that there was some resistance here but there is a greater problem overall. The equivalent series resistance electrode where the carbon coating touched the current collector was 77Ω whereas the ESR for the electrode where there was metal on metal contact was around 2Ω. This shows there was a high resistance that vastly decreased the performance of the electrode.

Once this resistance was eliminated the CV curve shown in figure 3.12 was not very rectangular and the currents achieved were still very low compared to previous tests performed by Swansea university for Enserv. One explanation to this could be shown in figure 3.13. In one of the repeat tests, one of the electrodes was being washed with deionised water after being tested some of the carbon coating was flaking off where it had been submerged in 0.5M sodium sulphate solution where the electrode had not been fully coated with epoxy resin. This figure shows that is its possible for this electrolyte to delaminate the original carbon coating off the aluminium which would damage the electrode and cause high charge transfer resistance. The chosen testing substrate was changed to nickel. Nickel foam was considered as well as it demonstrates high performances in literature [18] and does not have any reactions with the electrolyte within the testing voltage ranges however, this material was not chosen as it has a considerably higher price, and the aim of this project is to move towards a scaled-up mass manufacture of supercapacitors so using foamed nickel is a slight step back from this goal.

3.8 Conclusions of Materials and Methodology

In this chapter, materials and methodologies were presented; in particular, the formulation and preparation of activated carbon inks, adopted throughout this work, and the associated selection of a suitable current collector substrate. Preliminary tests on a commercially bought carbon coated aluminium substrate demonstrated the inadequacy of this substrate, due to delamination issues. Nickel substrate was found suitable and selected for use throughout the main body of the work

CHAPTER 4: Results of Kuraray YP-80F Carbon Testing

This Chapter explores the synthesis of various ink recipes using Kuraray YP-80F activated carbon as the active material, this carbon is originally characterised using SEM, Raman spectra analysis and particle size analysis. this carbon is then prepared into three different recipes of ink using various quantities of ethyl cellulose binder and subsequently electrochemically tested to measure performance.

4.1 SEM Characterization

A SEM image the plain Kuraray YP-80F sample is shown in figure 4.1. it shows particles sizes within the order of single numbers of microns. Figure 4.2 shows a SEM micrograph of the same carbon but at higher magnification with measurements of 14 random particles in random directions ranging from 710nm to 4.04μm these figures were. An electrode made from the 10% EC 11.25% Super P carbon black and 78.75% Kuraray YP-80F activated carbon ink was also micrographed giving figure 4.3. In this figure it is possible to see the particles that were sized in the order of microns. Surrounding each larger micron particle there

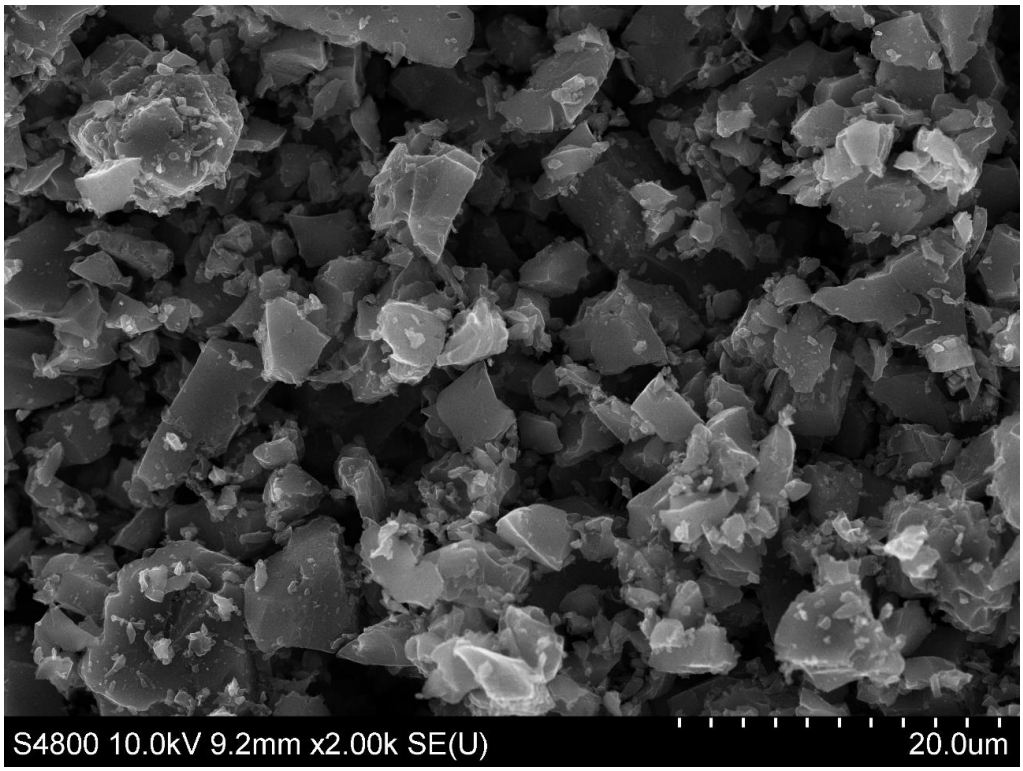

FIGURE 4.1:
SEM micrograph of Kuraray YP-80F activated carbon

are smaller particles, these are likely the smaller particles of conductive Super P carbon black. The fact that there are no agglomerations of these Super P particles implies the ink was well mixed before it was coated onto the substrate.

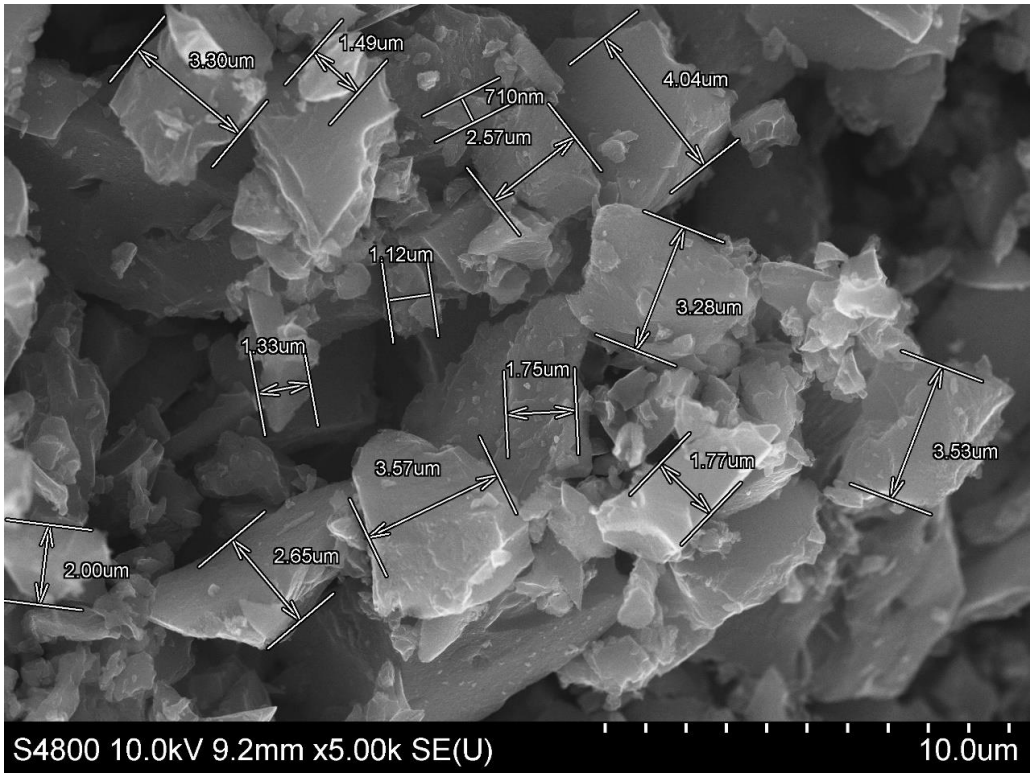

FIGURE 4.2:
SEM micrograph of Kuraray YP-80F activated carbon

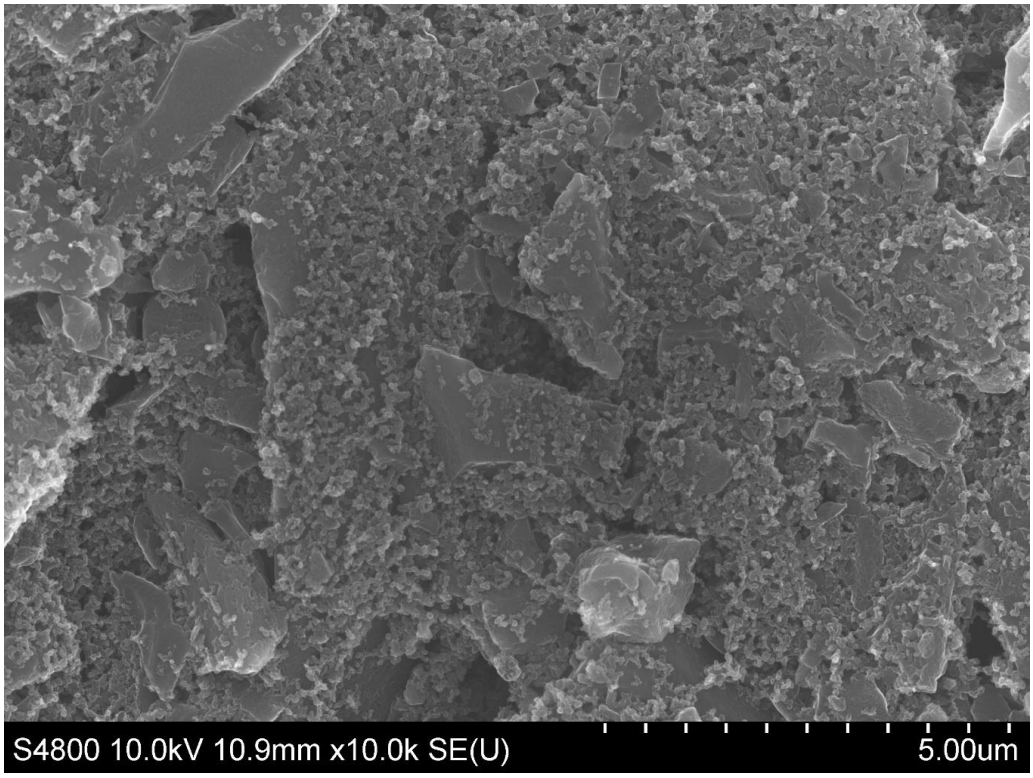

FIGURE 4.3:
SEM micrograph of Kuraray YP-80F activated carbon electrode using 10% EC ink recipe

4.2 Kuraray YP-80F Particle Size Analysis and Raman Characterization

The Morphology 4, the machine that gathers the Raman spectra, can also analyse particle sizes. This particle size analysis was performed on both the Kuraray YP-80F activated carbon and on Enserv's Super Carbon. Raman Spectroscopy was used to characterise the Kuraray YP-80F activated carbon, this is shown in figure 4.4. The spectra show peaks at 1330cm^{-1} (D) and at 1590cm^{-1}(G) and a distinct lack of a peak at 2700 cm^{-}1(D2). The two evident peaks show the presence of sp^3 and sp^2 bonds respectively, the sp^3 bonds are the conductive bonds within activated carbon and therefore the higher that peak's intensity the higher the conductivity of the carbon. As seen that peak's intensity is smaller than that of the sp^3 peak therefore this carbon isn't too conductive, therefore 1/8 of the carbon in the inks was Super P conductive carbon to increase the conductivity of the overall ink. Overall, this spectrum shows that this very stereotypically activated carbon.

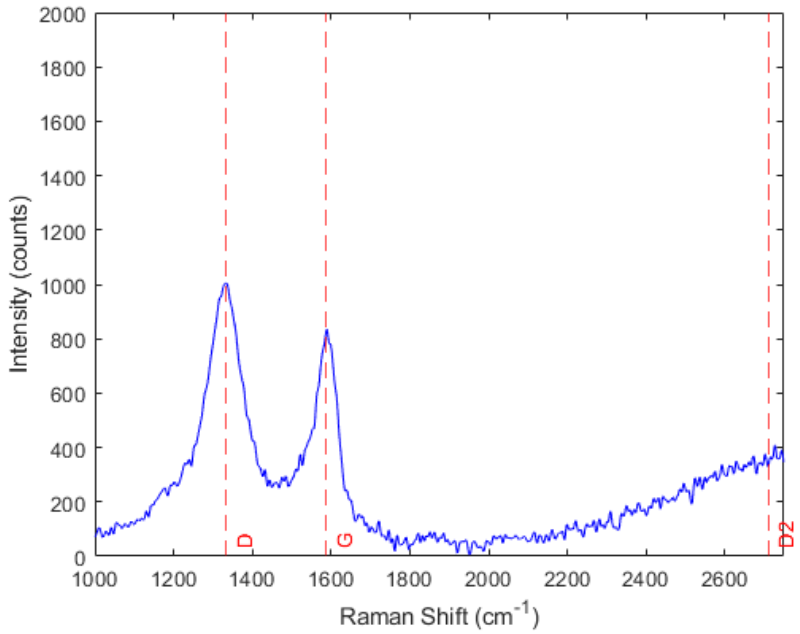

FIGURE 4.4:
Raman spectra of Kuraray YP-80F activated carbon

The particle size analysis performed using the same Morphology 4 machine is shown in figure 4.5, it shows a relatively well sorted array of particle diameters within the order of single numbers of microns with a few particles being higher than 10µm and even fewer being higher than 20µm. It should be noted that the scale for the particle diameter has a logarithmic scale therefore the grain sizes increase considerably.

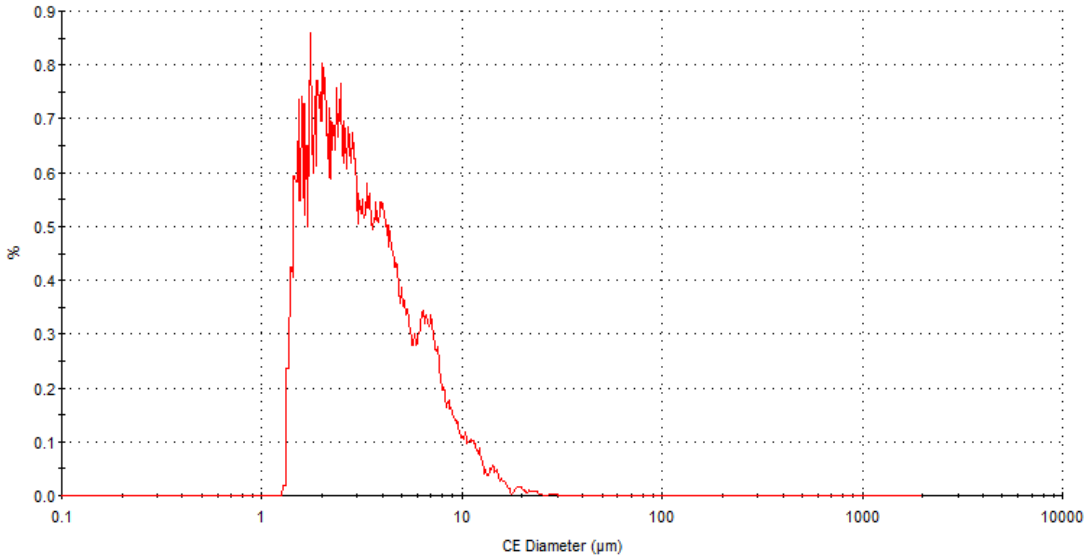

FIGURE 4.5:
Particle Size Analysis of Kuraray YP-80F activated carbon

4.3 3D Optical Microscopy Characterization

The electrodes were created by bar coating the synthesised ink onto the electrode surface. The bar coater used was a K Control Coater. The bar used to coat the ink onto the electrode is designed to coat 24μm of the wet material that will then dried in an oven overnight to form the electrode coating. This dried electrode coating was imaged using an Alicona 3D microscope that can image rough surfaces by collecting multiple images of an electrode at differing focal distances and stitching the images together to create a 3D image. Figure 4.6 shows the image of one of these 3D images of the 10% EC ink printed onto nickel. It shows the rough topology of the electrode surface.

FIGURE 4.6:
Optical microscopy 3D model of the 10% EC ink bar coated onto a nickel substrate

However, it is not possible to add any more information using this 3D model as there is no correct scale bar. It is however possible to use this 3D model to colour code an overhead microscopy image to display the height of the sample. This type of image is displayed in figure 4.7. it shows an area in the middle that is at a greater height than the areas in the top and bottom of the image. It should also be mentioned that the orientation of the sample in all the microscopy samples are perpendicular to printing direction. A less zoomed version of this figure is shown in figure 4.8. it shows that there are also peaks and troughs running parallel to the printing direction. The bar that was used to coat the inks onto the substrates was a threaded steel bar therefore the lines that are evident in these images are most likely from the threads on the bar leaving an imprint onto the electrodes.

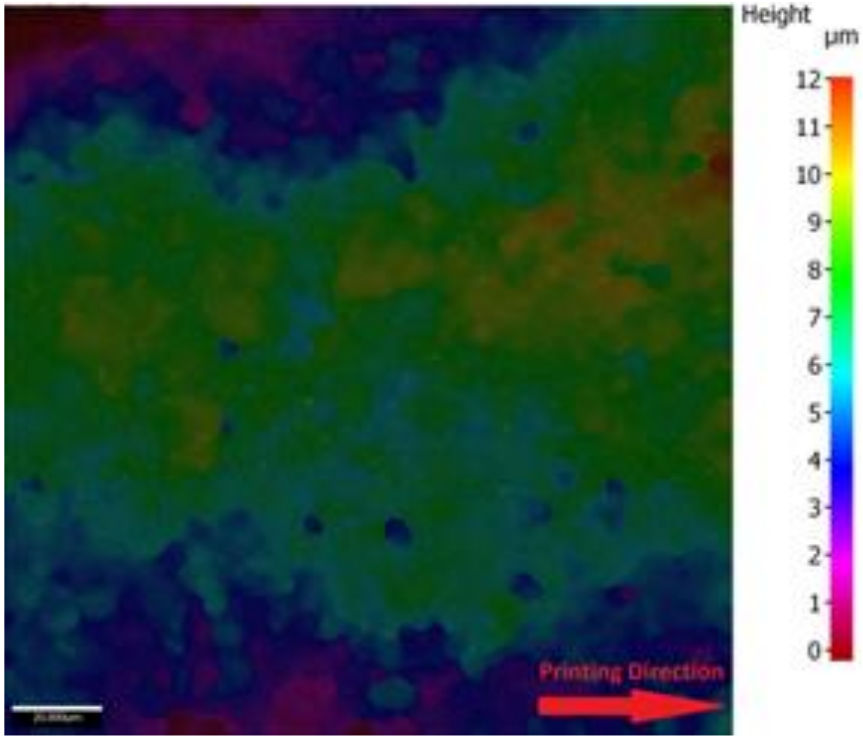

FIGURE 4.7:
3D microscopy image of the 10% EC ink bar coated onto a nickel substrate with colour coded height measurements

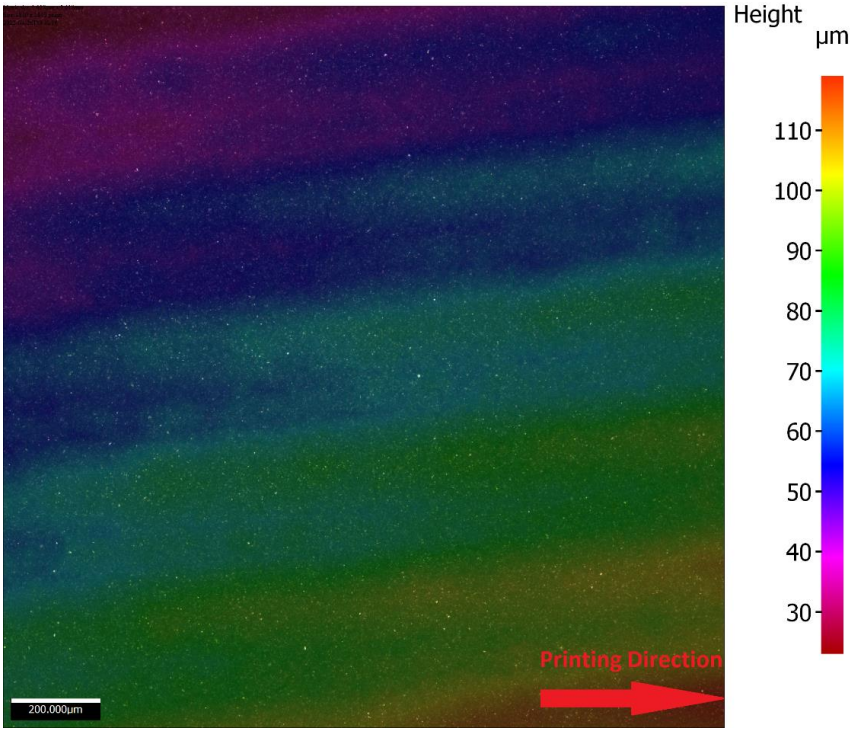

FIGURE 4.8:
3D microscopy image of the 10% EC ink bar coated onto a nickel substrate with colour coded height measurements

4.4 Electrochemical Evaluation of Kuraray YP-80F Electrodes

This section of the thesis focuses on the electrochemical results collected from the testing of the testing of the Kuraray YP-80F materials using various ink recipes. The ratios of each of the formulations were different depending on which test was being performed, each of these recipes can be seen in TABLE 3.1. These exact recipes were chosen by changing the percentage of ethyl cellulose to the quantities listed and keeping the ratio of the two different types of carbon at 7:1 Activated carbon to Super P carbon black.

	Weight percent of ingredient		
Name	Activated Carbon	Ethyl Cellulose	Super P
20% EC	70	20	10
10% EC	78.75	10	11.25
5% EC	83.125	5	11.875

TABLE 3.1
Recipes of various inks used to make and test activated carbon electrodes

Figure 4.9 shows multiple cyclic voltammetry curves from the 20% EC in printed on a nickel substrate. These CV curves are a lot closer to the classical capacitor square shape, even at higher scanning rates. The currents achieved in this test were considerably higher than the other tests performed on the carbon coated aluminium. The mean value for capacitance across

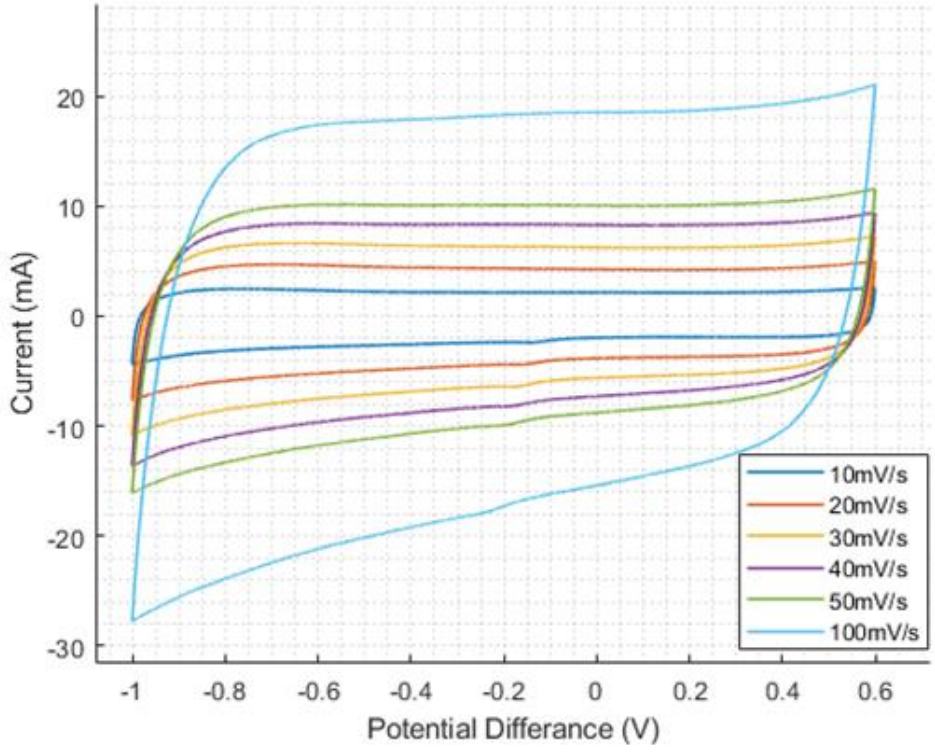

FIGURE 4.9:
CV plot of the 20% EC electrode using Kuraray YP-80F coated onto a nickel substrate

all these curves was 50.4F/g. using the multiple scan rates it is possible to plot the current at the same point on each curve against the scanning rate. This should give a linear set of data that can be fitted into a line of best fit to show a linear plot shown in figure 4.10.

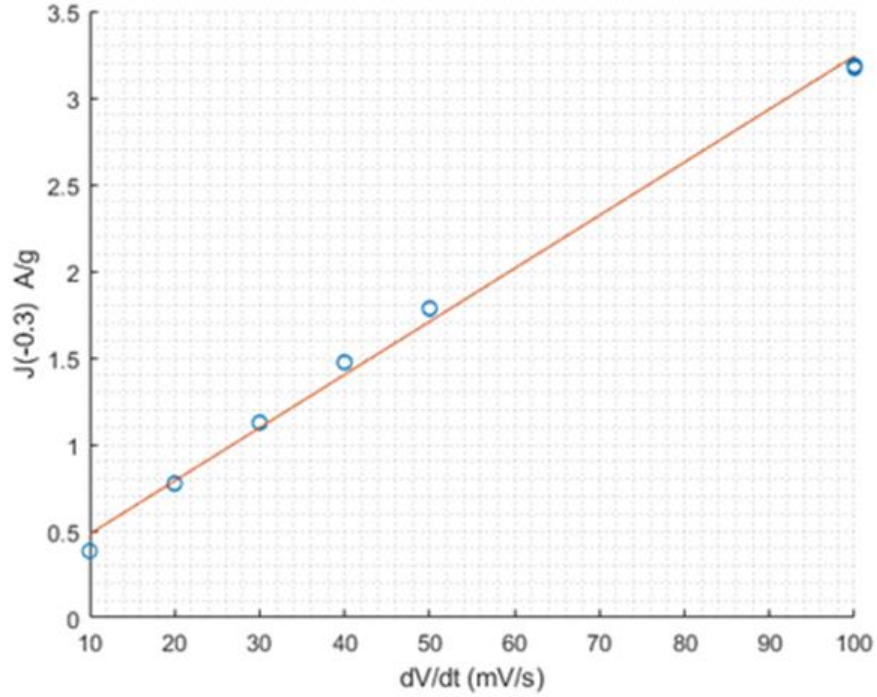

FIGURE 4.10:
Specific current Vs scanning rate of the 20% EC electrode using Kuraray YP-80F coated onto a nickel

Figure 4.11 shows the GCD plots for the 20% ink on nickel at varying current scan rates, it is immediately apparent that the plots now look a lot more triangular than the previous GCD plots. Another thing to note is that as the current rates increase, the time it takes for the voltage to both increase and decrease to the set values decreases. It is also noted that the first 10mA/s plot takes considerably longer than the other five cycles. Also, as the currents increase, the voltage jump starting at -1V increases. This is as expected as this voltage jump is directly proportional to the internal resistance of the electrode which remains constant compared to the currents

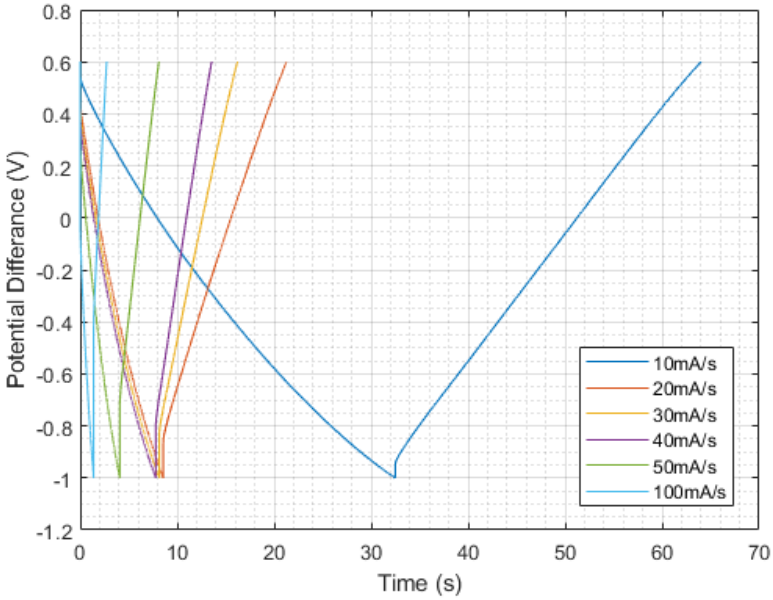

FIGURE 4.11:
GCD plot of the 20% EC electrode using Kuraray YP-80F printed on a nickel at varying scan rates

The coulombic efficiency is plotted against the specific current in figure 4.12 this graph shows a rather stable coulombic efficiencies at all the currents tested starting at 95% at 0.99 A/g and finishing at 89% at 9.93 A/g. the error bars in this figure were calculated using the 5 repeats of each test under the same conditions. The voltage jumps of these curves both at the

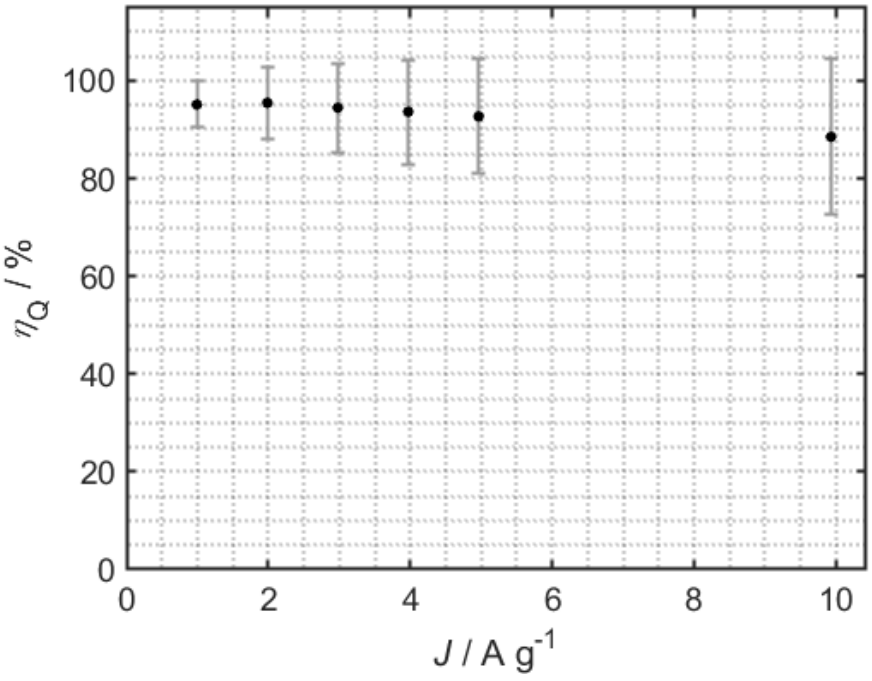

FIGURE 4.12:
Coulombic efficiency vs specific current of the 20% EC ink in a nickel substrate

top and the bottom of the GCD plots are plotted against the specific current of the GCD plot in figure 4.13. This shows that both the top and bottom voltage drops are similar and have a linear relationship with the specific current. The internal resistance of the cells can be calculated with these plots. The higher voltage drop gave an ESR of 2.62 Ω and the bottom voltage jump gives an ESR of 2.12 Ω.

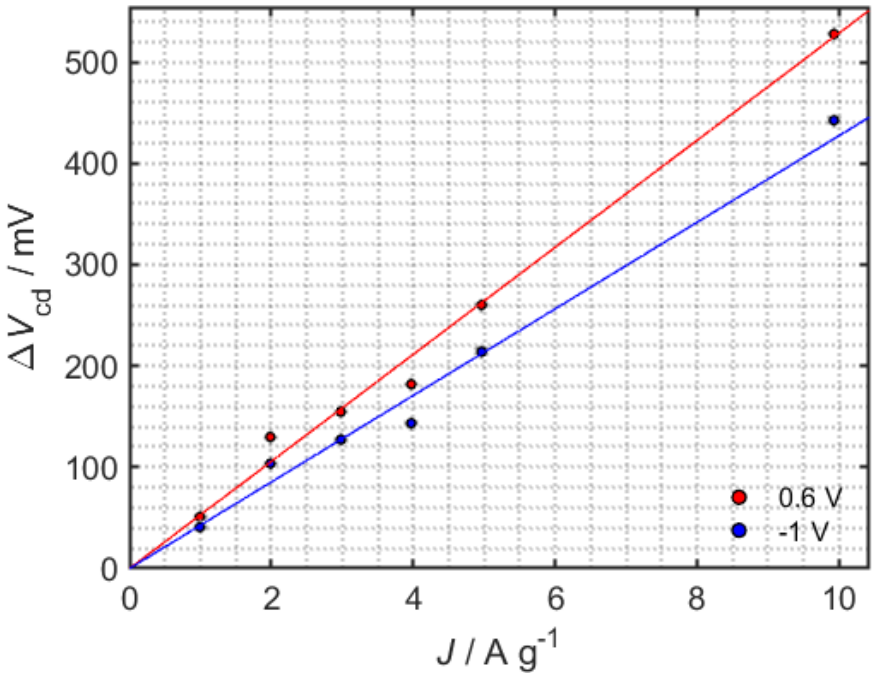

FIGURE 4.13:
Change in voltage at 0.6V and -1V due to internal resistance of electrode vs specific current of the 20% EC ink in a nickel substrate

It is also possible to calculate the specific capacitance using the GCD graph. The capacitances per gram were calculated for each of the tests and plotted against the current densities. This is shown in figure 4.14 these results show that the initial specific capacitance tested at 1.0A/g started off with a specific capacitance of 28.9 F/g however this relatively high specific capacitance decreases as the current density increases the specific capacitance decreases finishing off with 16.55 F/g at 9.9 A/g demonstrating that this electrode's performance is limited at higher currents.

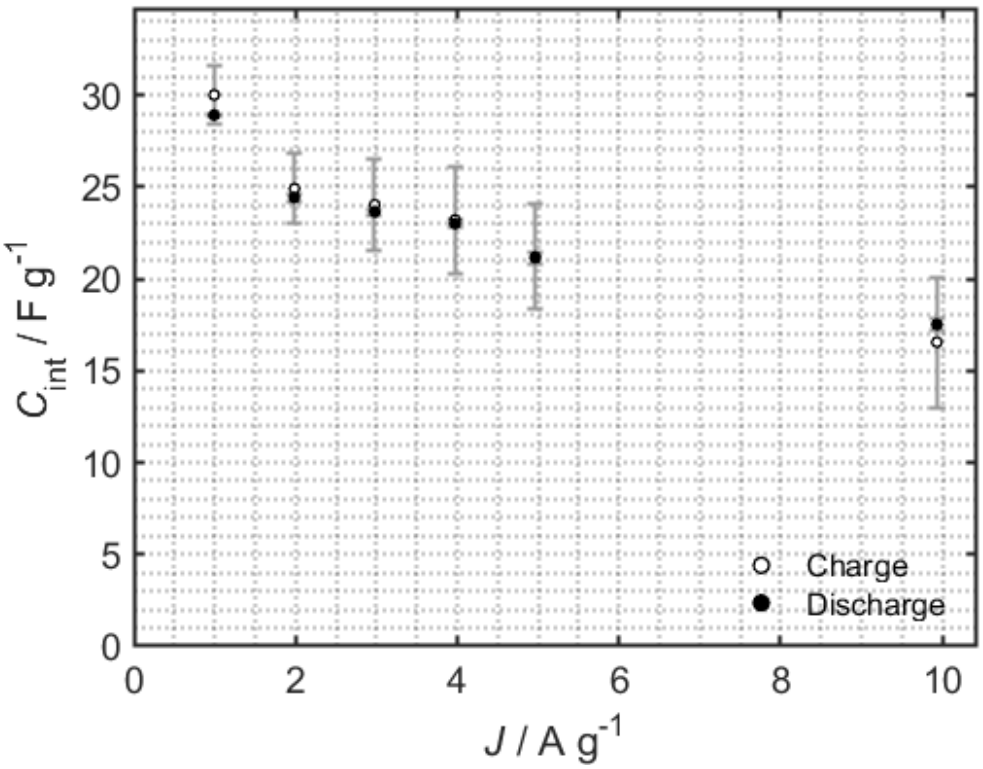

FIGURE 4.14:
Specific capacitance vs specific current of the 20% EC ink in a nickel substrate

Finally, the EIS scan for this 20% EC ink electrode at varying voltages is shown in figure 4.15. At higher frequencies there is a small protruding flat semicircle before the 45^{O} angle that does not change with voltage, this means that there is a resistance that arises from the interfacial resistance that is not correlated to charge transfer. The ESR in this graph is also slightly smaller than previous EIS plots at 1.42Ω which is smaller but still within the same order of magnitude so not that different.

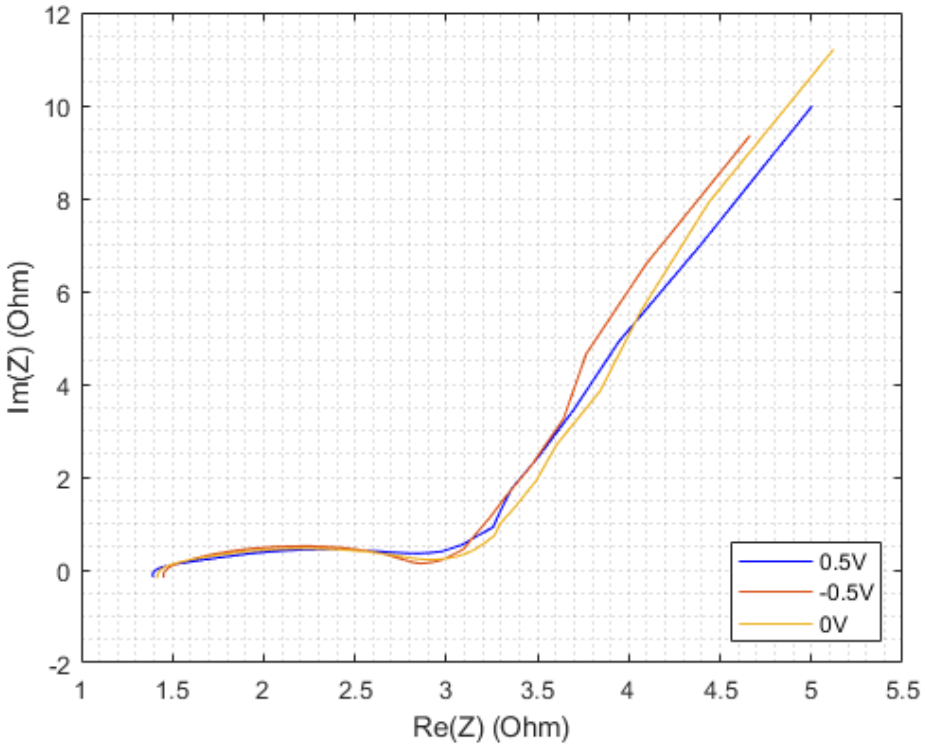

FIGURE 4.15:
EIS plot of the 20% EC electrode using Kuraray YP-80F printed on nickel

The CV graph with all the scan rates recorded for the electrode made by coating the 10% EC ink is shown in figure 4.16. Up until 50mV/s, the shape is very much the classical supercapacitor like rectangular shape however, this changes when it gets to the 100mV/s, the rectangular like shape smoothens out and an oval shape with a point is produced indicating a decrease in performance due to higher energy loss because there is a higher current. As previously mentioned, the capacitance of the 10 V/s curve was calculated to be 64.1 F/g. The linear graph shown in figure 4.17 illustrates a linear relationship between the current at a defined voltage of -0.3V on discharging and the voltage scan rate. The final datapoint on this graph is considerably lower which is most likely due to the higher currents within the electrode which creates a higher resistance and therefore worsens the performance.

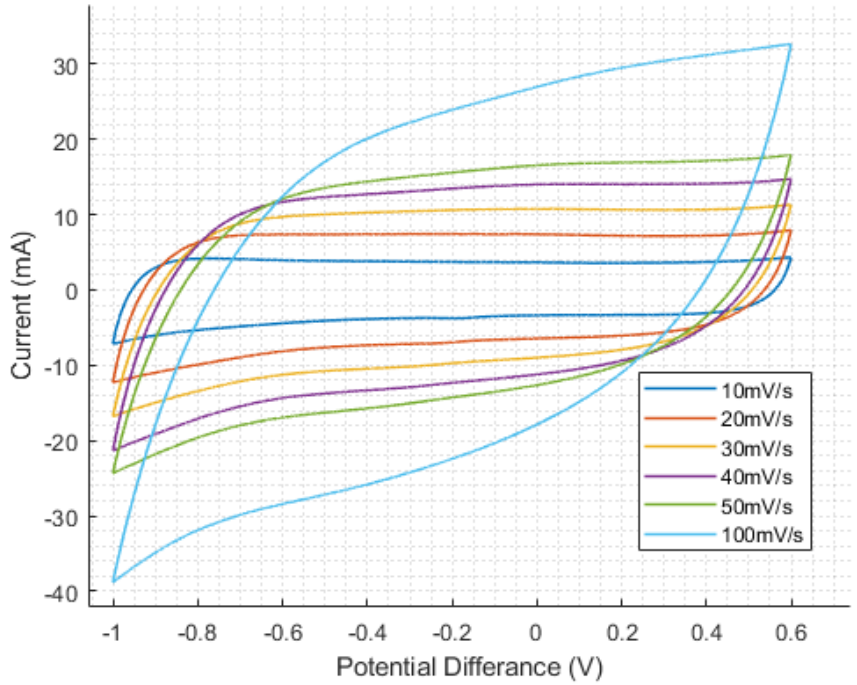

FIGURE 4.16:
CV plot of the 10% EC electrode using Kuraray YP-80F coated onto a nickel substrate

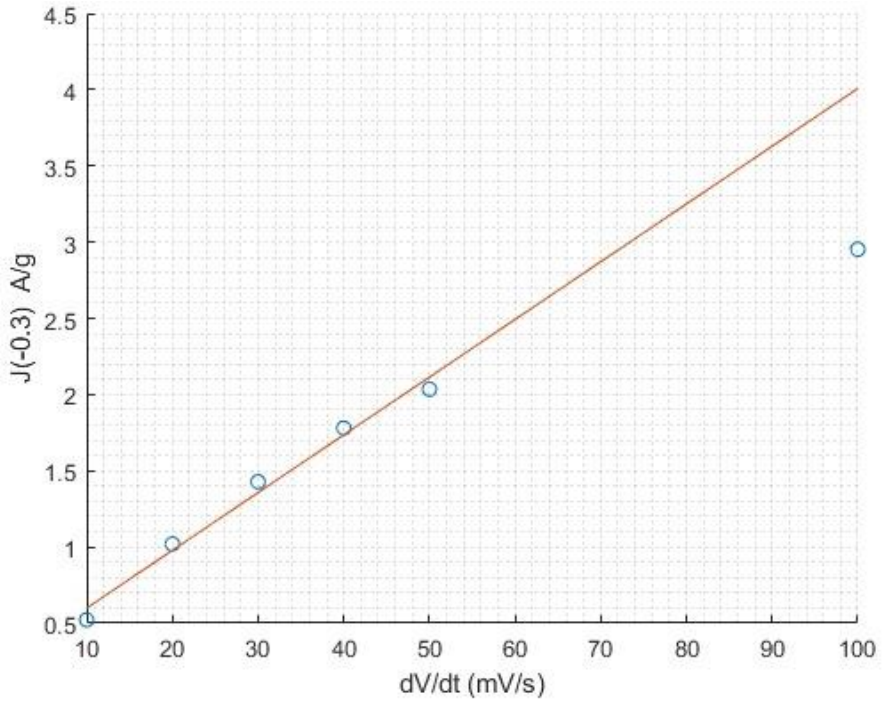

FIGURE 4.17:
Specific current Vs scanning rate of the 10% EC electrode using Kuraray YP-80F coated onto a nickel

The GCD for the 10% EC electrode coated on nickel is shown in figure 4.18. This GCD curve shows multiple GCD plots at different scan rates and as the current rate increases the time to charge and discharge decreases until the 100mA/s where it takes a longer amount of time to charge the 100mA/s than it did to charge the 50mA/s. However, on discharge the 50mA/s plot took longer. The ESR of this graph was calculated to be 2.8Ω. Using the GCD data, the graph for columbic efficiency against the specific current is shown in figure 4.19. The coulombic efficiency decreases as the specific current increases starting at 95% at 1.38A/g and ending at 81% at 13.76A/g. Finally, the voltage drops at both minimum and maximums and these are plotted against the specific current of the electrode as shown in figure 4.20. The plot shows that the voltage jump at positive ends of these GCD graphs are bigger than the voltage drops at the negative ends and therefore the electrode loses more energy at the positive voltage section as the internal resistance is higher at this end. As the gradient of these curves are directly proportional to the internal resistance of the electrodes it is evident that the resistance is higher at 0.6V and lower at -1V. these resistances have been calculated to be 4.02Ω and 2.77Ω respectively.

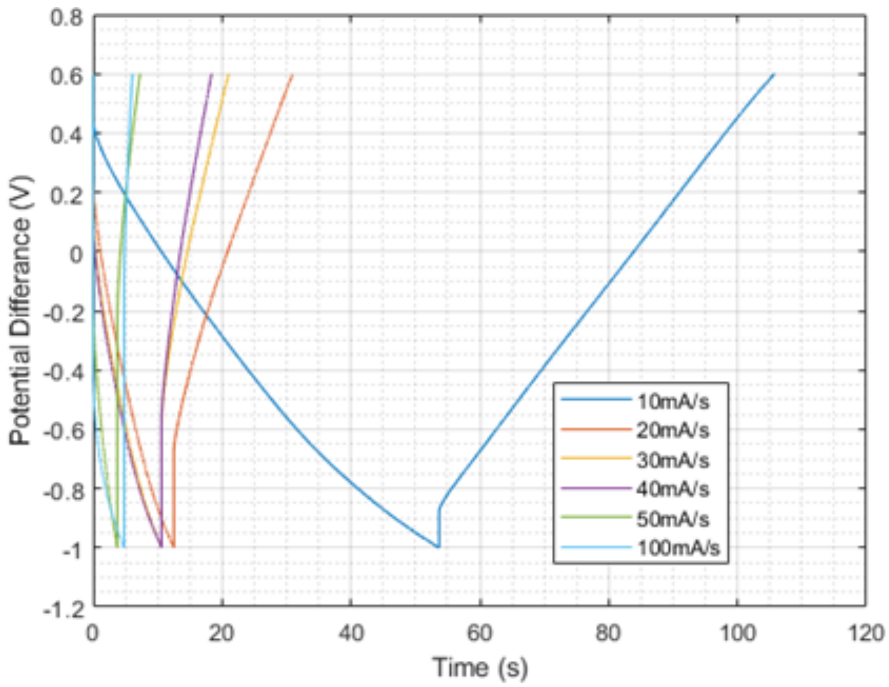

FIGURE 4.18:
GCD plot for the 10% EC ink coated on nickel at multiple current scan rates

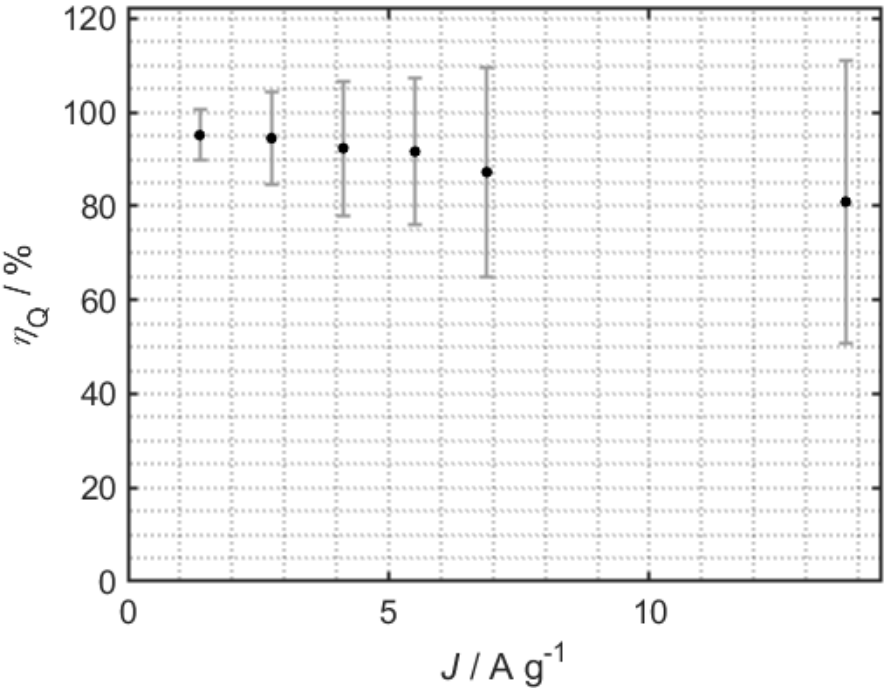

FIGURE 4.19:
Coulombic efficiency plot for the 10% EC ink coated on nickel

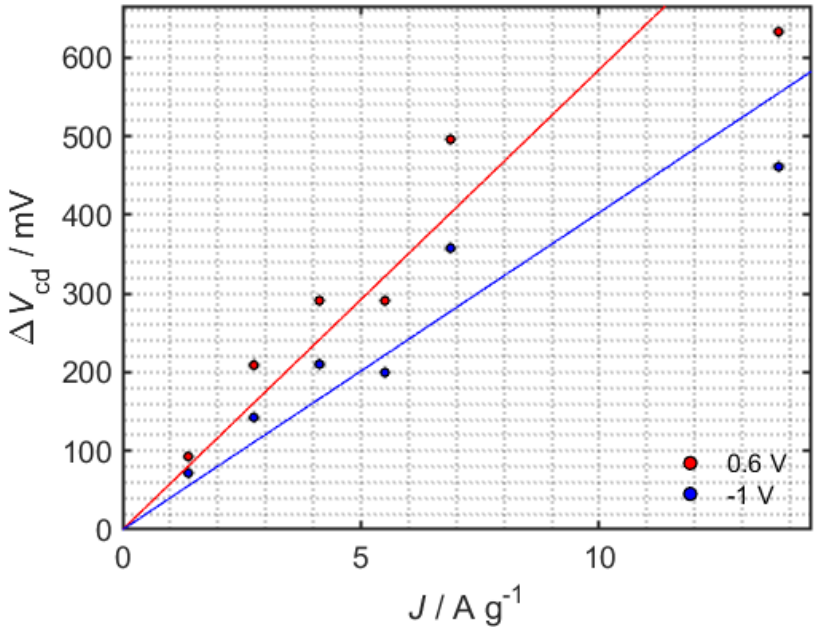

FIGURE 4.20:
voltage drops at both minimum and maximums are plotted against the specific current for the 10%EC electrode

The specific capacitances were also calculated using the GCD plots and plotted against the specific currents as shown in figure 4.21. this figure shows a relatively high starting specific capacitance of 62.3F/g at 1.4A/g. however, this high capacitance decreases considerably at

higher currents leading to 23.5F/g at 13.8A/g which is still outperforming the 20% EC ink but not as much at this higher current.

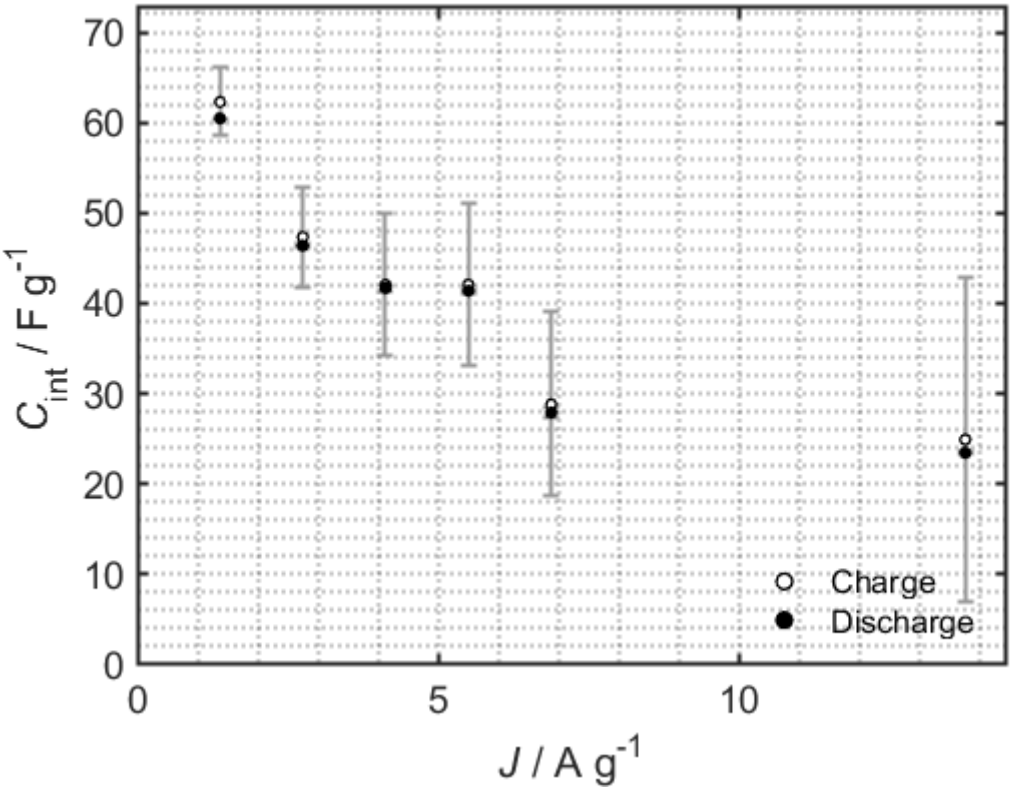

FIGURE 4.21:
specific capacitance vs specific current of the 10% EC ink in a nickel substrate

The EIS plots for this 10% EC electrode are shown in figure 4.22, it portrays three plots with large semicircles that vary with respect to the voltage illustrating that the resistance is correlated to charge transfer. Another point of note is that the average ESR is 2.0V with the ESR of the -0.5V plot having a higher resistance. As the resistance is still comparatively low the charge transfer resistance is not an issue and most likely arises from the charge transfers of electrons within the electrode.

The final ink recipe to be tested was the 5% EC ink on nickel. The CV curves of three different voltage scan rates for this electrode are shown in figure 4.23. It again shows a set of rectangular CV curves however at higher and lower voltages the curves start to peak this can be evidence of oxygen or hydrogen evolution. On these specific curves the currents achieved were overall less than the 10% EC reaching a specific capacitance of 23.0F/g when tested at 10mV/s.

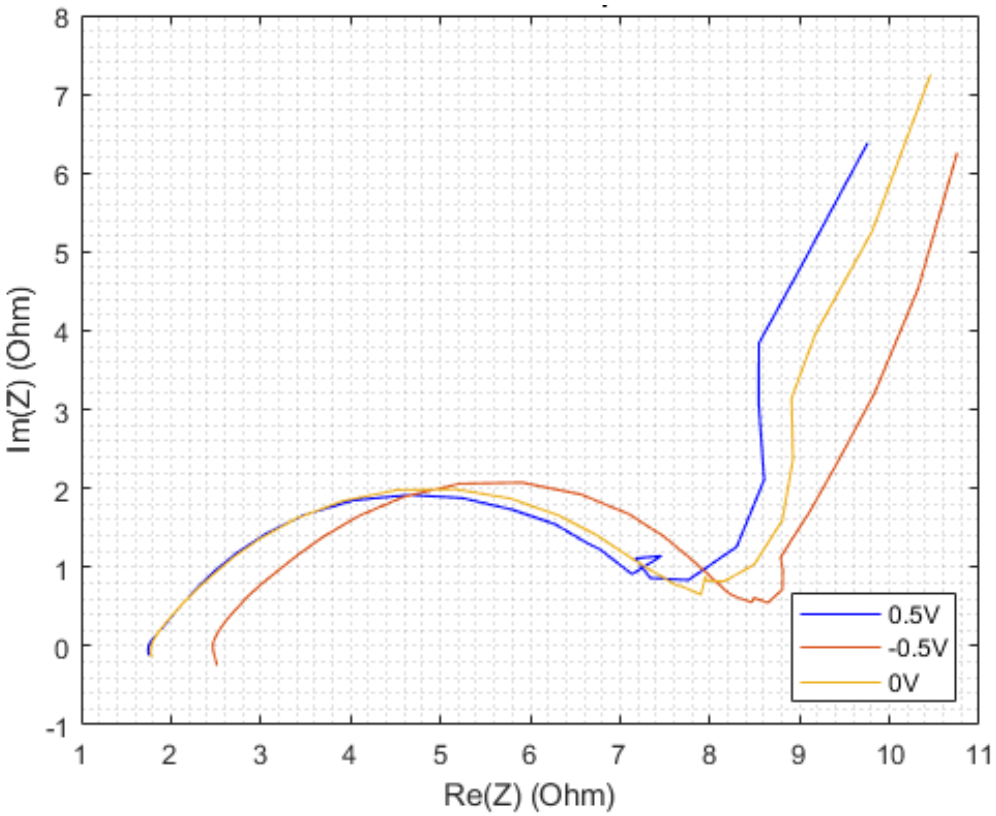

FIGURE 4.22:
EIS plot of the 10% EC ink at varying voltages

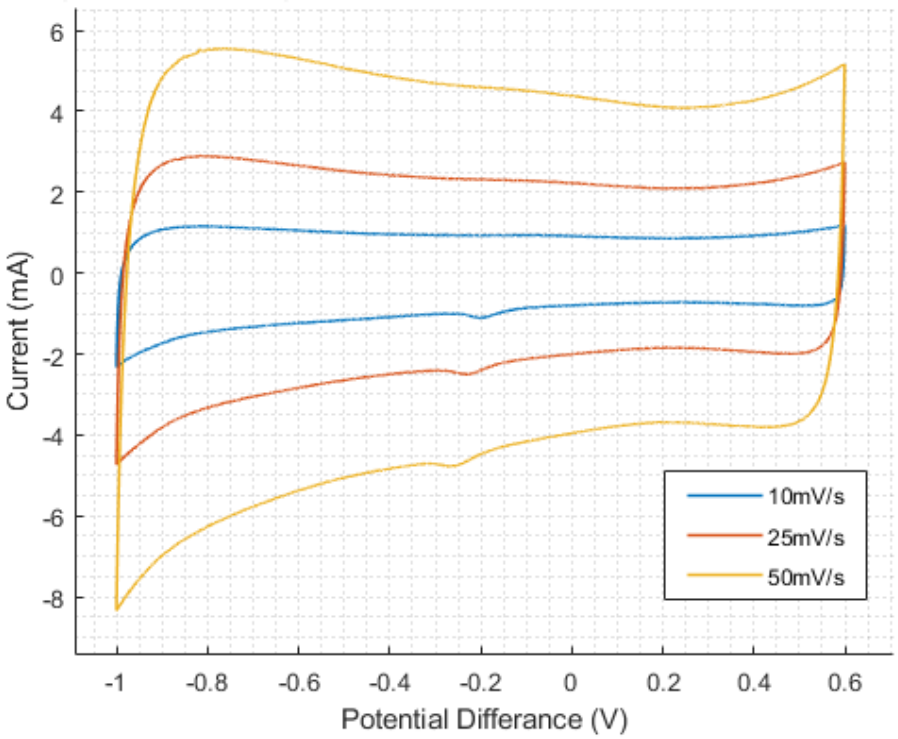

FIGURE 4.23:
CV curve of the 5% EC electrode using Kuraray YP-80F printed on nickel at varying scan

The GCD graphs for three of the GCD curves at various currents for the 5% EC on nickel are shown in figure 4.24. Again, all the plots are very triangular with voltage jumps against the specific currents that are shown in figure 4.25, the gradients of these linear plots are proportional to the ESR of the electrode. The ESR at 0.6V is 2.66Ω and the ESR at -1V is 1.55Ω. Finally, the coulombic efficiencies of these plots are shown against the specific currents in figure 4.26. it shows a somewhat stable coulombic efficiency graph starting at 96.6% at 1.9A/g finishing at 94.5% at 9.5A/g. this 96.6% at 1.9A/g is close to 100%. It would be impossible to have exactly 100% efficiency due to resistance in the system losing energy however getting as close to 100% is possible and important as it decreases the energy loss of storing energy in these devices.

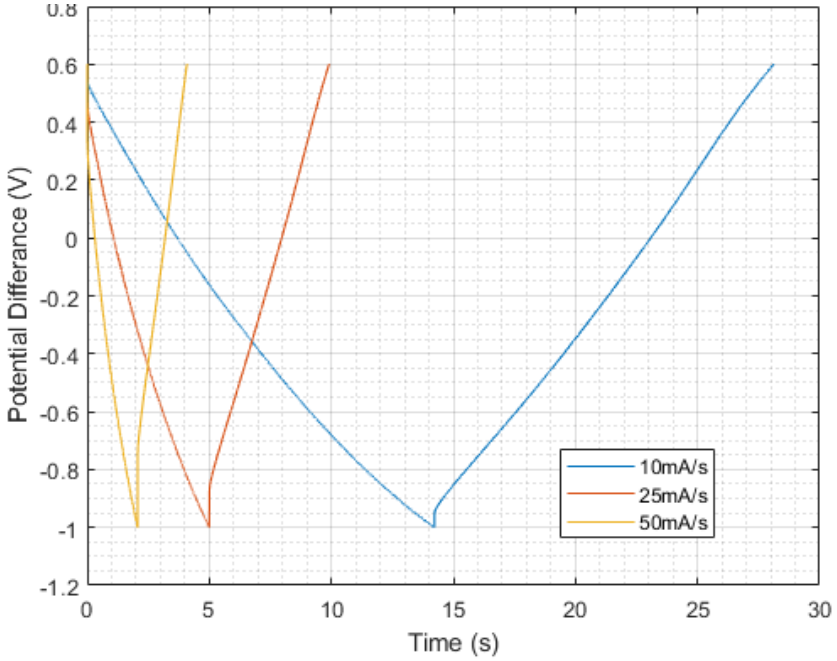

FIGURE 4.24:
GCD plot of the 5% EC electrode using Kuraray YP-80F printed on a nickel at varying scan rates

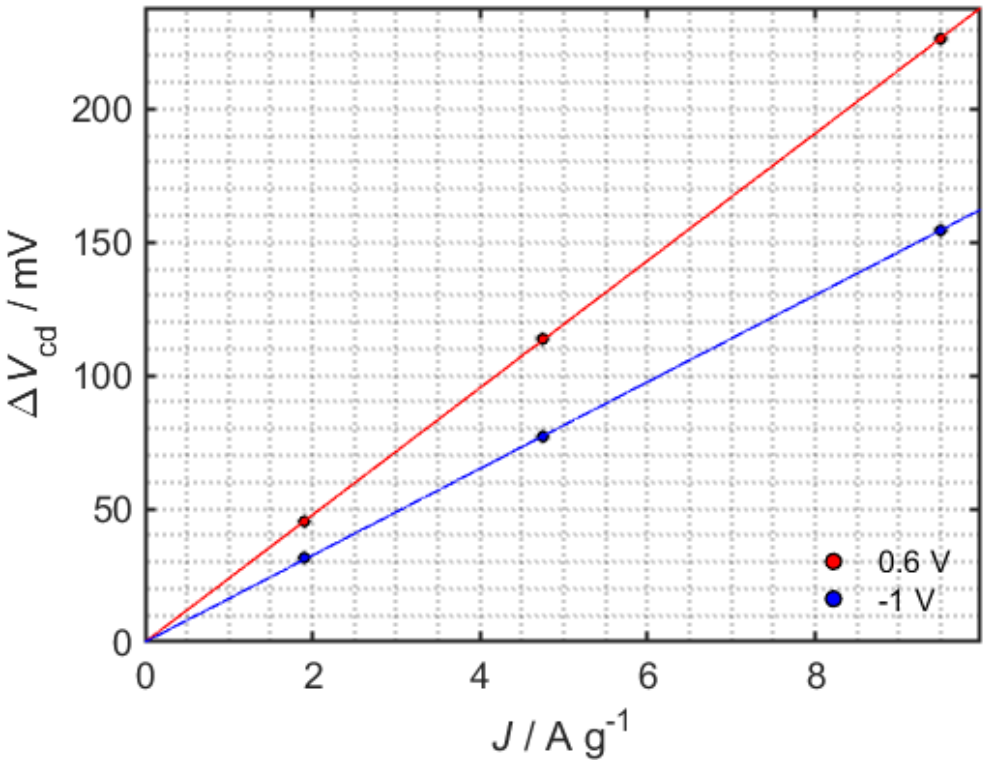

FIGURE 4.25:
Voltage drops at both minimum and maximum voltages plotted against specific currents for the 5% EC electrode

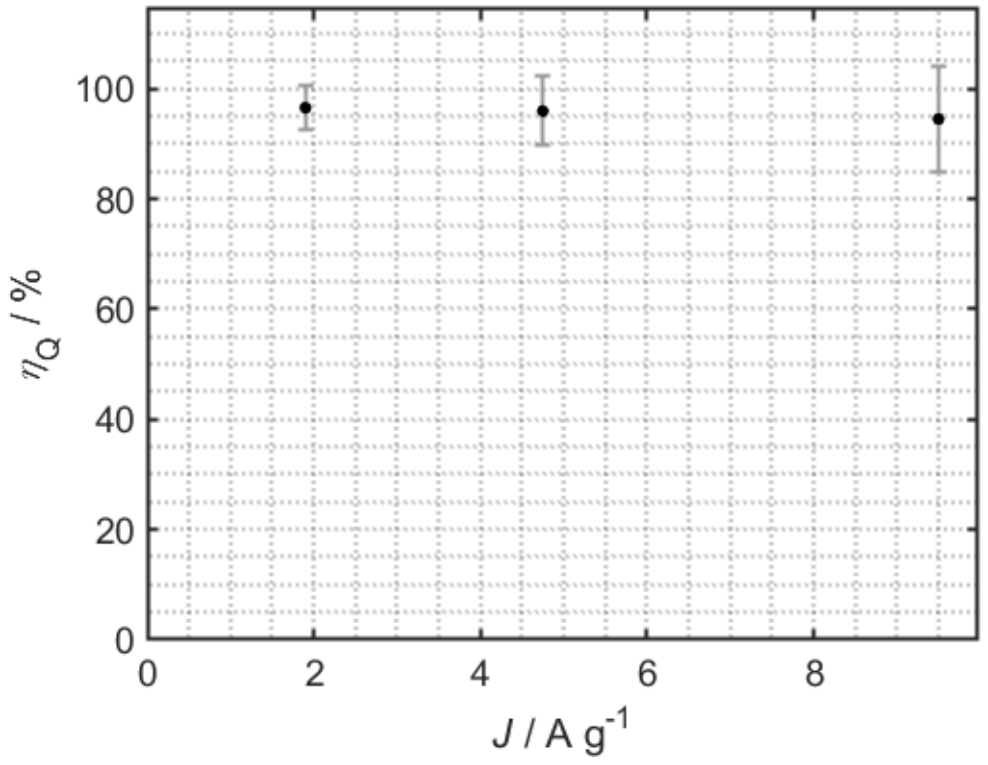

FIGURE 4.26:
Coulombic efficiency vs specific current of the 5% EC ink on a nickel substrate

The specific capacitances were calculated using each GCD test and were plotted against the specific currents. The specific capacitances of this test were considerably worse than the previous two electrode ink recipes starting at around 17.4F/g at 1.9A/g and ending at 9.5F/g at 13.7A/g which shows considerably worse performance than both of the two previous recipes printed on nickel

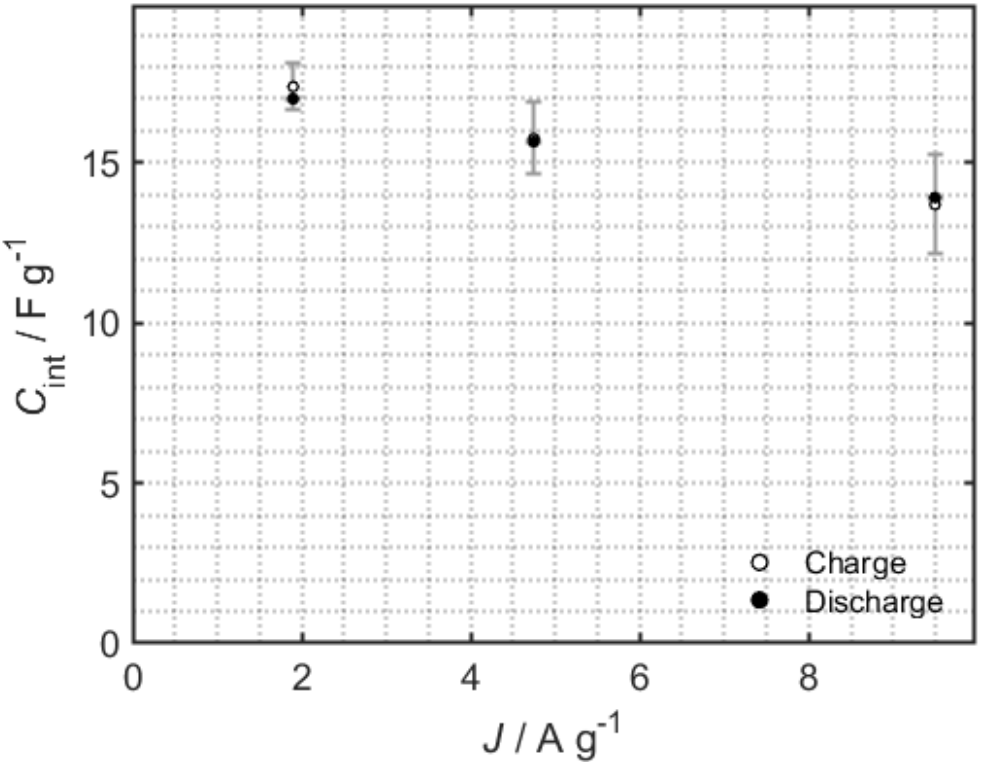

FIGURE 4.27
Specific capacitance vs specific current of the 5% EC ink in a nickel substrate

Finally, the EIS plots for this 5%EC electrode are shown in figure 4.28. At the starting point of these plots, the ESR has an average of 1.1Ω. The higher frequency end of the plot does not have an evident semicircle but would probably have more of a semicircle at a different scale of the high frequency region implying a there is some resistance in this electrode arises from charge transfer. more of a flat line before it hits the 45^{O} angle going into the lower frequency range.

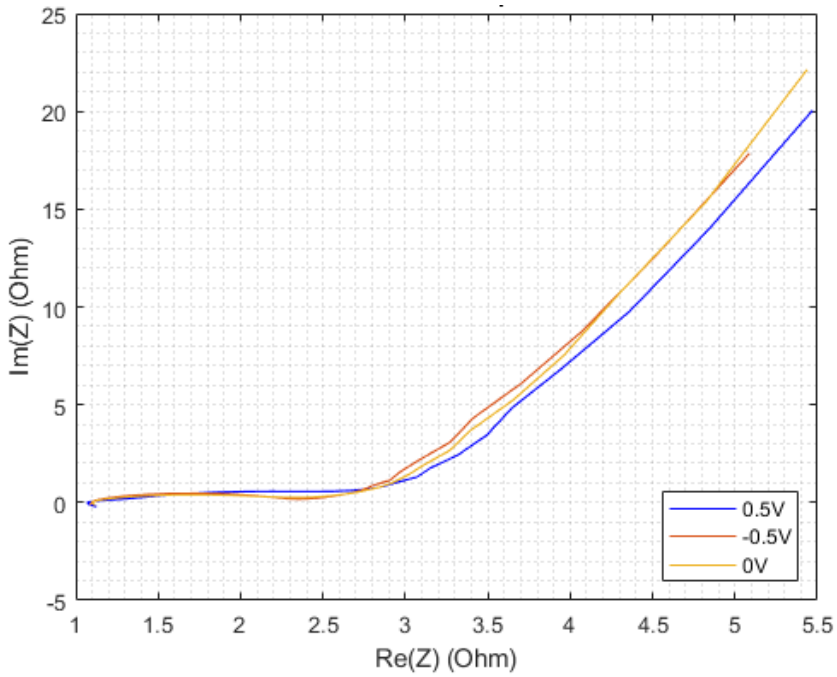

FIGURE 4.28:
EIS plot of the 5% EC electrode using Kuraray YP-80F printed on nickel

4.5 Anomalous initial test of 10% EC ink recipe

The next electrode made was the 10% EC ink coated on nickel. The original test showed promising results. Figure 4.29 shows the CV curve for this original test, it shows a very rectangular shape with a very large area which gives a calculated specific capacitance value of 114F/g. However, if this same CV curve is compared to the CV curves of the other two repeats

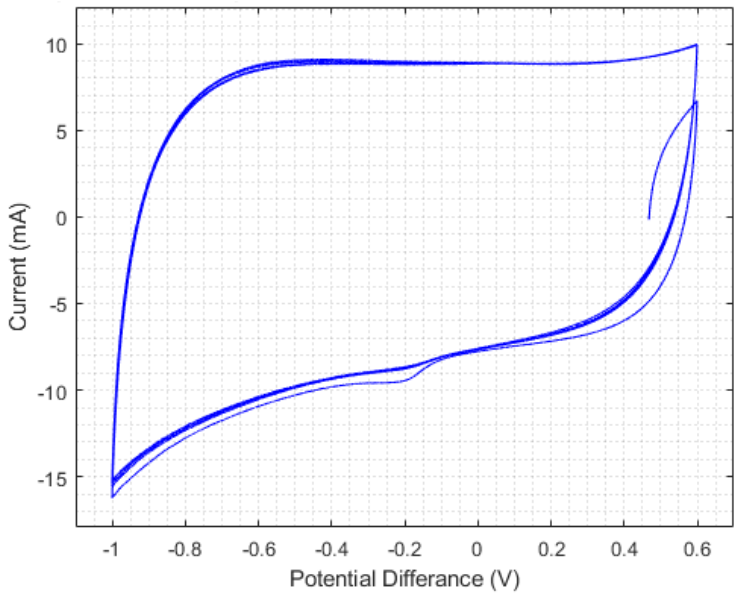

FIGURE 4.29:
CV plot of the 10% EC electrode using Kuraray YP-80F coated onto a nickel substrate

that were done with this ink and the currents corrected to currents per gram of electrode material (shown in figure 4.30) this shows the two other repeats having a much smaller specific capacitance at around 64.1F/g when tested at 10mV/s. This result gives the impression that the first test was anomalous and therefore only the repeats will be used to evaluate the performance of the 10% EC electrode coated on nickel.

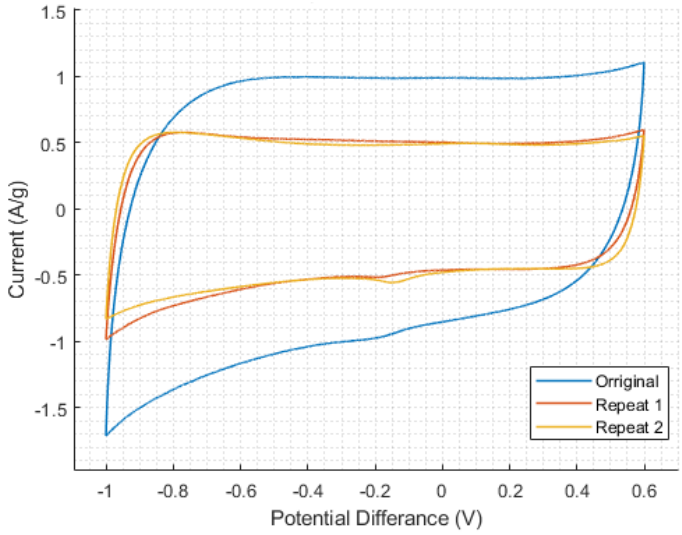

FIGURE 4.30:
CV plot of the 10% EC electrode using Kuraray YP-80F coated onto a nickel substrate showing all 3 repeats

4.6 Discussion of the characterisation of the Kuraray YP-80F Activated Carbon

The SEM characterisation of the Kuraray YP-80F activated carbon shows a well sorted particle system with a high surface area material with particle sizing varying between 1µm and 10µ. This is also shown in the particle size analysis graph sown in figure 4.5 which shows most of the particle's diameters of the Kuraray YP-80F to be in the order of a number of microns with particles ranging from just over a micron to just over 20 microns. The size of the carbon particles can have a large effect on the performance of the electrodes they create as the smaller the particle sizes the higher the surface area of the carbon. An increase in surface area is generally good for the performance of the supercapacitor electrode as there is a more space for the carbon to be stored. Because this is an activated carbon material these particles are all porous carbon with holes into electrolyte infiltration through the entirety of the carbon, however if the particle sizes get too big, there is a possibility that the electrolyte will not fully infiltrate the sample and cause dead mass within the electrodes that is not useful for storing

energy. The sorting of the carbon particles can theoretically be important for the performance of the electrode. If the particles are poorly sorted, meaning there is a variety of different particle sizes, the electrode will have a higher density compared to an electrode which is better sorted which will be comparatively less dense. The density of the electrode can have an effect on both the ion intercalation, (how well the ions soak into the electrode and find areas to be stored), and the conductivity of the electrode, (if the particles are too spread apart, the resistance of the electrode will be considerably higher because electrons could have getting to the current collector).

The Kuraray YP-80F was also Raman tested to verify the type of carbon being used and to check for any impurities. The spectra gathered, figure 4.4, shows this Raman spectra presenting two distinct peaks and the lack of an overall peak. The first peak shows the presence of sp^3 bonds, which is the same type of covalent boning that occurs in diamond, and the second peak shows the presence of sp^2 bonds. The sp^2 bonds are the bonds that are more conductive therefore the larger this spike the higher the conductivity of the electrode. This shows that the electrode could be more conductive if this sp^3 peak were higher than the sp^2 peak. The conductivity of this carbon was already known to be poor, therefore the Super P was added into the ink mix to increase the conductivity and allow the current to flow through the electrode. The lack of an overall peak indicates the bond that is associated with graphene, graphene is a good conductor however is not very capacitive and therefore would not be useful in a supercapacitor electrode.

The way that the electrode material is coated onto the substrate can affect the performance of the electrode as it controls how much material is deposited onto the electrode and the surface texture of the electrode. The aimed wet surface thickness was set to be around 50 μm, and this was set as a control variable that was always kept the same. The bar that coated 50 μm of wet material had threads on it, the imprint of these threads can be seen from the surface micrographs shown in section 4.1 these lines could help by either giving more surface area of the electrode to allow more area for electrolyte infiltration or later hinder the supercapacitor by removing space where electrode material could be once the full cell is assembled. However, as this threaded 50μm bar was kept as a control variable this was not within the scope of this project.

4.7 Discussion of electrochemical performance of Kuraray YP-80F Electrodes

The 20% EC ink that had previously been used in different projects was a good starting recipe for the optimisation of the ink recipe. The performance of the 20% EC ink on nickel showed similar performance to the previous testing of these getting a specific capacitance of 50F/g at 10mV/s scan rate after 2000 cycles. The shape of the CV curve for this test has a rectangular shape much like a classical supercapacitor should have even at higher voltage scan rates. The currents at -0.3V were plotted against the current density and the fact that this has a linear relationship even at the higher current shows that this electrode was still relatively stable at this scan rate as the current density should be proportional to the current at a set voltage if the electrode is stable and that this electrode can perform well around 100mV/s. The GCD testing overall showed good performance giving coulombic efficiencies of 95% for lower current densities to 89% at higher current densities meaning that the energy output was 95-89% of the energy that was put in, all the coulombic efficiency values are shown in figure 4.12. All GCD plots looked very triangular with the only exception being the voltage jump at both the upper voltage limit and top voltage limit. As stated previously, these voltage jumps each indicate the internal resistance of the electrode which can be calculated using the amount of voltage that has been jumped and comparing that to the current at testing. These voltage jumps are compared to the currents at this electrode in figure 4.13 as the internal resistance of each electrode is calculated by dividing the voltage dropped at these points by the current it was tested at, the equivalent series resistances are directly proportional to the gradients of these lines, as seen in the graphs, there was a higher resistance at the higher voltage limit compared to the lower. These resistances were calculated to be 2.62Ω at 0.6V and 2.12Ω at -1V. the EIS graph can be used to help understand the source of these resistances. The Specific capacities for the 20%EC electrode shown in figure 4.14 shown in figure show a capacitance starting at 28.9F/g at 1.0A/g, these capacitances steadily decrease until reaching a final capacitance of 16.55F/g at 9.9A/g. The EIS plot for this graph is shown in figure 4.15, in the higher frequency region, it shows a drawn-out semicircle that is not affected by voltage meaning there is a small amount of interfacial resistance that is not proportional to charge transfer. This means that there is some resistance at the interface, but this resistance is not affected by charge transfer. A possible reason that the resistance is not proportional to charge transfer is because this is the electrode with the most binder in it, it was well adhered to the nickel substrate therefore there was not an issue with charge transfer, there was however a small amount of interfacial

resistance due to 20% of the dry material being made up of ethyl cellulose, a non-conductive polymer that would create resistance within the electrode. the equivalent circuit resistance, for this electrode is given by the real impotence at the starting x intercept, for this 20% EC ink on nickel, the average ESR of the -0.5V, 0V and 0.5V tests was 1.42Ω.

The 10% EC ink also showed good performances. The CV curves for one of these electrodes are shown in figure 4.16. it shows some classically rectangular CV curves for the curves between 10V/s and 50V/s however in the final 100V/s the CV curve is more of a pointed ellipse that is rotated anticlockwise. However, compared to the previous 20% EC ink sample the currents achieved in all the tests were better, this is shown with the fact that the overall capacitance per gram for this electrode using a 10mV/s scan rate was 64.1F/g which compared to the same value of 50.0F/g meaning that the 10% EC ink was certainly better than the 20% EC ink at lower voltage rates and therefore at lower currents. However at higher voltage scan rates the rectangular like CV curve is not shown, there is still a large area in this curve but the classical supercapacitor like rectangular shape is not shown meaning there will be some lost performance in this test. This lost performance can be seen in figure 4.17. As shown the first five plot points show a very linear system. However, at the final point, the 100mV/s test, the current for this datapoint is considerably lower than the linear model, which shows the performance of this electrode is limited at higher current densities. The GCD performance also tells a similar story. At first glance, the GCD plots shown in figure 4.3.11 do show some triangular plots with a similar voltage drop as in previous GCD graphs however this time the voltage drops have a larger drop for each test compared to the 20% EC ink electrodes in figure 4.11. The coulombic efficiencies plotted against current densities in figure 4.19 show a similar level of performance compared to the 20% EC ink when comparing the at lower current densities with the plot starting at 95% efficiency however at the higher current densities the efficiency drops down to 81% at 13.8A/g. When the high voltage jumps shown in the GCD plots are plotted against the specific current in figure 4.20, this produces a much steeper gradient than the same figure for the 20% EC ink electrode and as the gradients are proportional to the internal resistance of the cell the resistances are higher than the 20%EC ink electrode. These resistances were calculated to be 4.02Ω at the 0.6V limit and 2.77Ω at -1V which is as previously mentioned, higher than the 2.62Ω and 2.12Ω of the same measurements made using the 20% EC ink electrode. This shows that the 10% EC ink electrode had a similar resistance at -1V compared to the 20% EC ink electrode but at higher voltages the internal resistance increased. The EIS plots for this electrode show an average equivalent series resistance of 2.0Ω.

As well as that, the presence of a large semicircle represents an interfacial resistance. The diameter of this semicircle is roughly the value of this resistance, meaning there is a large interfacial resistance in this circuit. It has also been noted that the semicircle shifts with changing potential which means this interfacial resistance is correlated to charge transfer. The only variable that has changed in this figure compared to the previous electrode is the reduction in binder and therefore the presence of an interfacial resistance is not surprising as there has been a reduction in the amount of the material that attaches the electrode to the current collecting material meaning the resistance increases as the active material is not transmitting its charge easily to the current collecting material. Comparing this 10% EC ink electrode to the 20% EC ink electrode, the 10% EC ink electrode has better capacitances per gram at lower current densities however at higher current densities the capacitance, efficiency of the 10% EC ink electrode drops due to an increase in interfacial resistance that varies with current meaning at high currents the resistance increased.

Finally, the third type of electrode was the electrode that was made using the 5% EC ink on a nickel substrate. The overall performance of this electrode was worse than that of the 10% and 20% EC ink electrodes. At lower voltage scanning rates the overall performance was 32.0F/g. The overall shape of these electrodes' CV curves was overall very rectangular and supercapacitor like but did start to peak when getting to higher and lower voltages, when using an aqueous electrolyte these peaks often show that the electrolyte is separating causing a hydrogen or oxygen evolution when the voltage is too low or high respectively. The GCD curves for this graph demonstrates that all the tested current densities show a triangular shape indicating that the charge and discharge both had relatively equal performance. The efficiencies of these tests are shown in figure 4.26 illustrating the coulombic efficiencies against the current densities of these tests. What this figure shows is that in the current densities tested the coulombic efficiencies barely decrease as the current density increases, however these tests were not as rigorous as the previous tests due to time constraints and therefore the extent of the performance at higher currents is unknown. The resistances in the electrode shown by the voltage drops at the upper and lower limit are shown in figure 4.25. This shows that the voltage drops for the positive limit increases more as current densities increase compared to that of the negative limit meaning there is a higher resistance at the positive end of the GCD curve compared to the negative end. The resistances calculated using these voltage drops and the specific capacities of the tests were 2.66Ω and 1.55Ω for the 0.6V and -1V jumps respectively. These values are in the same order as the previous electrodes tested and are comparable. The

final figure analysed for this electrode was the EIS graph for the 5% EC ink electrode on nickel. It shows a flat line in the high frequency region of the graph moving into an immediate 45^{O} angle that does not stop. It is noted that the graphs do not really change at all with voltage meaning that the resistances of this electrode are not proportional with charge transfer. This suggests that the electrode did not have a problem transmitting charge to and from the potentiostat and the decrease in performance of this electrode is to do with the electrode material not performing very well, this could be because the electrode was not as densely packed because the binder that stuck the material together had decreased. Because the material was not as densely packed there could have been material that was not in contact with the current collecting electrode and therefore dead mass that was not helping the performance of this electrode.

To conclude this section, the best electrode recipe created was the 10% EC electrode recipe that got a maximum capacitance of 62.3 F/g when tested at 1.4A/g. the second-best electrode was the original 20% EC electrode which demonstrated a lower specific capacitance all around but was much more stable at higher current densities. The final electrode tested; the 5% EC electrode was with worst performing electrode with low specific capacitances at even the smallest tested current densities. Previous literature that has tested a Kuraray YP-80F AC, poly-tetrafluoroethylene (PTFE) binder and C65 from Timcal® carbon black in a 90:5:5 ratio in an aqueous electrolyte normally shows specific capacitances around 90F/g. however, the literature found does use different testing conditions for example A.Platek et al [19] tested a Kuraray YP-80F electrode using a 1M LiOH electrolyte and a current density of 0.1F/g and obtained a capacitance of 90F/g. although these two measurements cannot be directly measured due to different testing conditions, this shows that the 10% EC electrode tested in this thesis works on the same order of magnitude as an electrode that is being tested in a current density an order of magnitude lower. Another example is that N.Kostoglou et al [20] produced a Kuraray YP-80F using a 10% PTFE 90% YP-80F electrode tested using a 1M CsCl electrolyte and scanning rate of 0.5mV/s which again would produce a lower current as the lowest scanning rate for CV in this thesis is 10mV/s which still got a specific capacitance of 64.1F/g.

In conclusions, the results evidence that a 10% concentration of EC appears to provide the best performance with a specific capacitance of 62.3 F/g when tested at 1.4A/g, in line with capacitance observed in literature with other polymers. It is evident therefore that EC appears a potential good polymer (adopting DAA as solvent) combining performance with ease of management/manufacture.

CHAPTER 5: Preliminary analysis of Enserv Super Carbon

5.1 Introduction to Enserv Super Carbon

Enserv has produced a type of high surface area carbon through a proprietary and confidential process and have asked That it's performance is tested within the synthesised ink recipe. This Chapter first characterises the carbon particle sizes then evaluates the electrochemical performance of this material through the same testing methods as the Kuraray carbon testing.

5.2 SEM Evaluation and Particle Size Analysis of Enserv Super Carbon

After testing the ink recipes using the commercially available Kuraray YP-80F, it was now time to test the performance of Enserv's Super Carbon. The carbons were first characterised using an SEM and then electrochemically evaluated using both the 10% EC recipe and the 5% EC recipe. Similarly to the Kuraray YP-80F, Enserv's super carbon was also micrographed using an SEM. A micrograph of just the Super Carbon is imaged in figure 5.1. This figure shows a poorly sorted array of different sizes of particles. Figure 5.2 shows a more magnified micrograph with ladled particle sizes. It shows a large disparity of particles ranging from 6.18μm to 44.2μm.

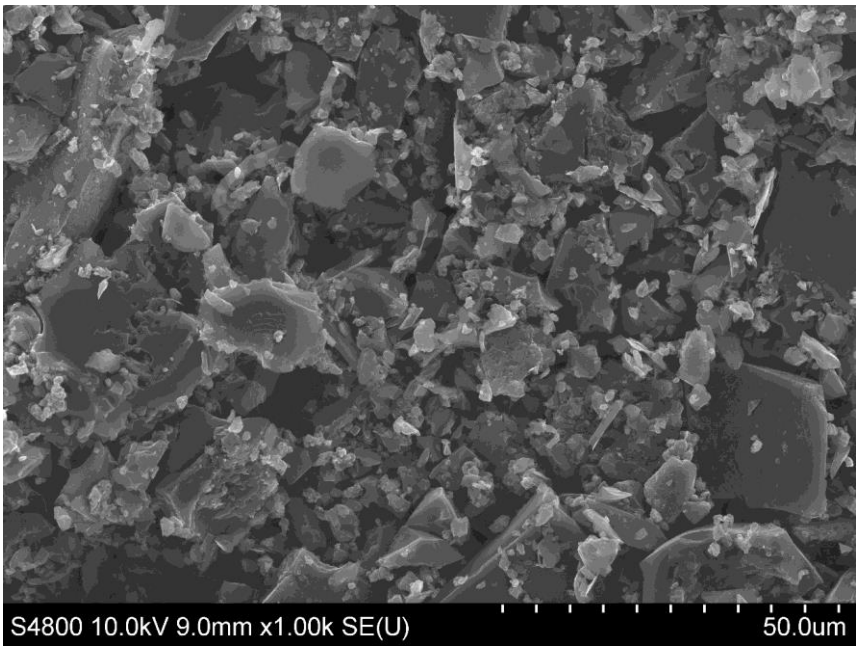

FIGURE 5.1:
SEM micrograph of Enserv's Super Carbon

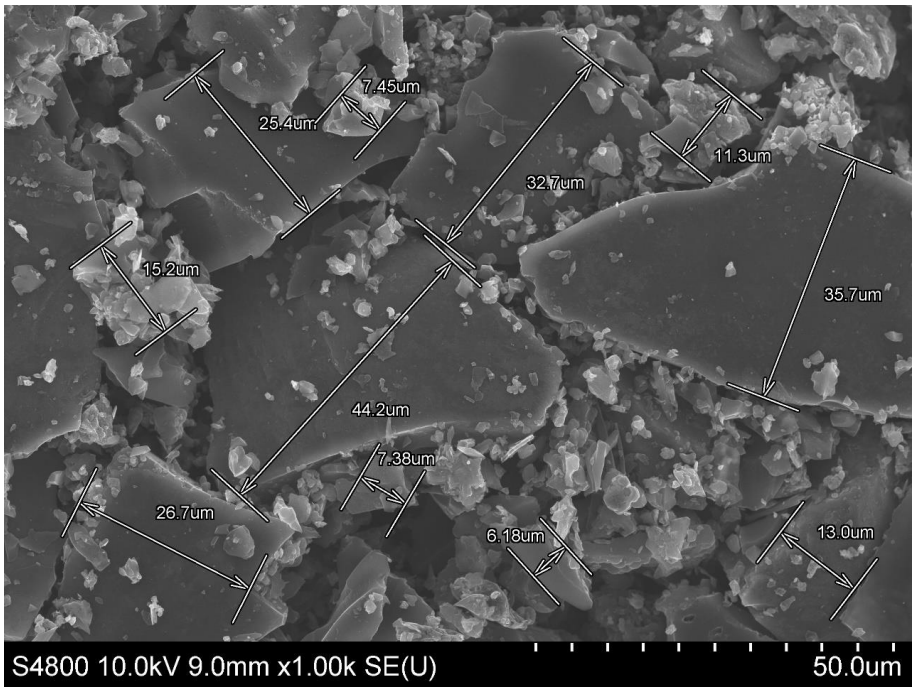

FIGURE 5.2:
SEM micrograph of Enserv's Super Carbon with labelled particle diameters

The penultimate SEM micrograph, figure 5.3, shows a micrograph of an electrode using the 10% EC recipe using Enserv's Enserv Super Carbon as the activated carbon. The figure shows the carbon particles with diameters in the order of tens of microns this ink has been mixed in a pulverisette ball mill and therefore the larger particles could have been milled down and made smaller, however as shown in the figure there are still carbon particles around 50μm diameter. Because of the magnification in this image, the Super P nanoparticles are not able to be seen as any higher magnification would not properly show the larger sizes of the carbon particles. The final SEM micrograph, figure 5.4, is a image of the same sample as figure 5.5 but at a much large magnification where the Super P particles are visible, it is evident that these super P particles are not agglomerating either and therefore this ink was mixed well enough to have a good homogeneity.

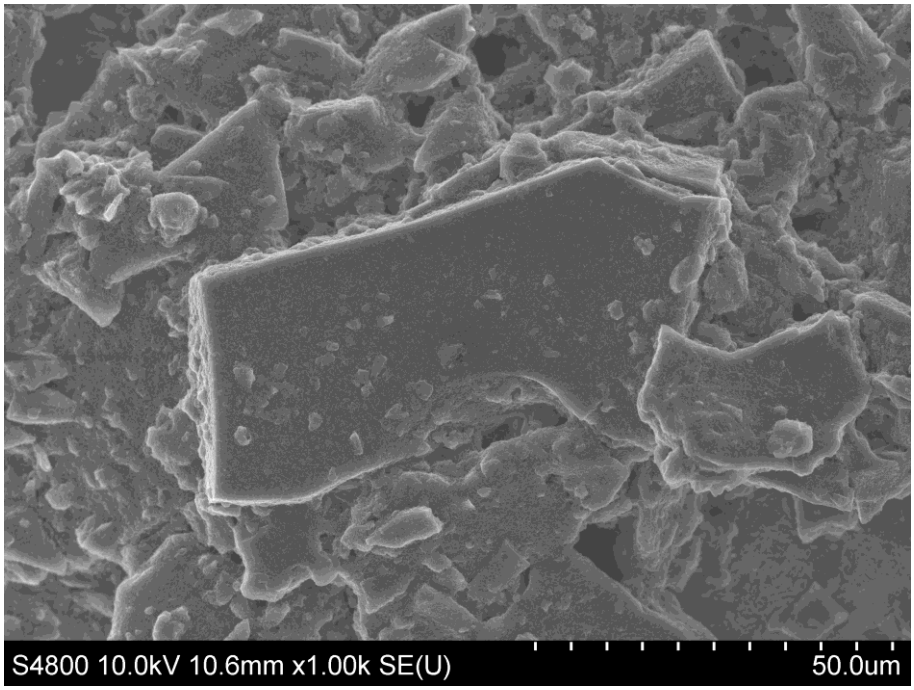

FIGURE 5.3:
SEM micrograph of Enserv's Super Carbon electrode using 10% EC ink recipe

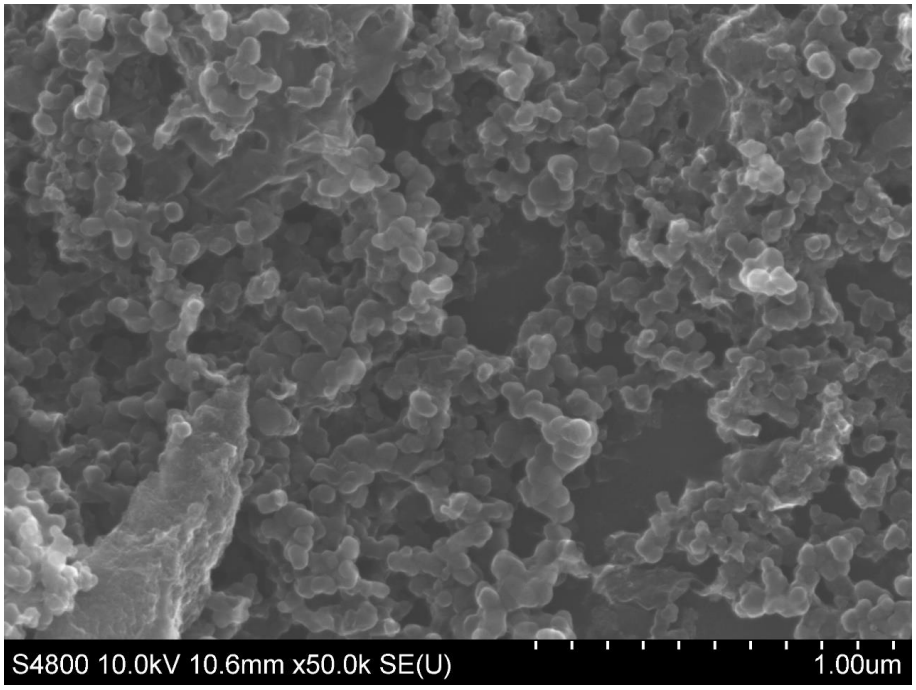

FIGURE 5.4:
SEM micrograph of Enserv's Super Carbon electrode using 10% EC ink recipe showing the presence of the super P conductive carbon

Figure 5.5 shows the particle size analysis chart for Enserv's super carbon. It does show the vast majority of carbon particles having diameters between 1-10μm however compared to figure 4.5. the peak for Enserv's super carbon is wider and trails into the 10-100μm portion

meaning there are more particles that have larger diameters. This graph has a logarithmic scale and therefore the grains get considerably bigger the further to the right they are meaning the little bumps around 100µm can be very large particles that can ruin the printing method, especially when the desired coating thickness is at an aimed 50µm.

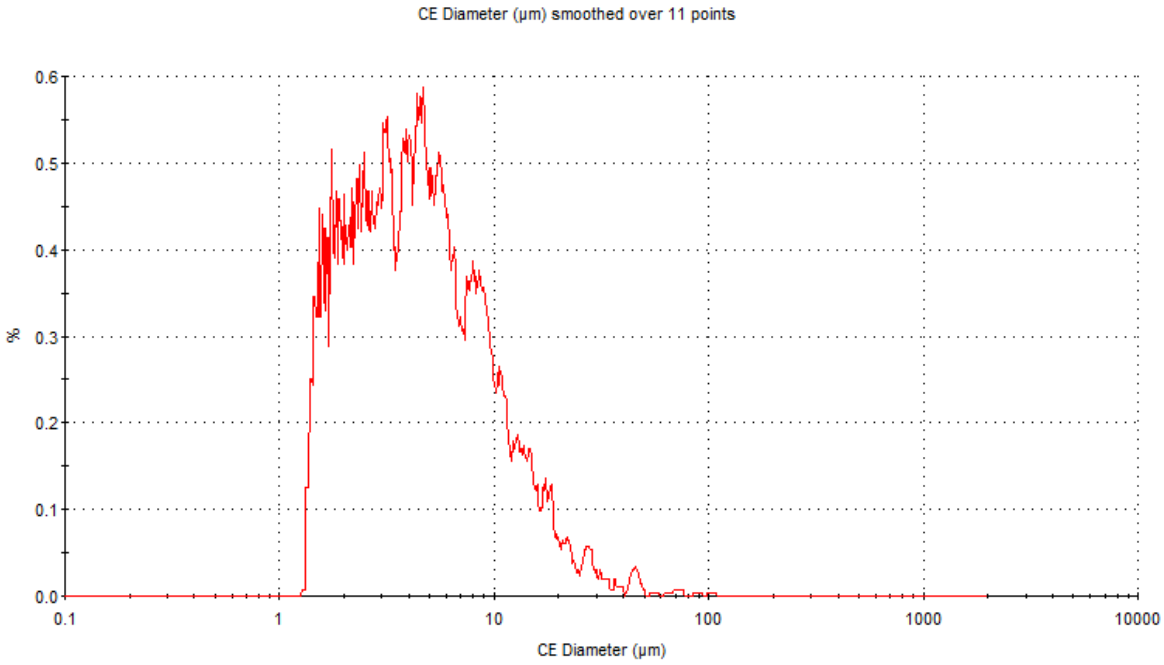

FIGURE 5.5:
Particle Size Analysis of Kuraray YP-80F activated carbon

5.2 Electrochemical Analysis of Super Carbon

This carbon is made by the carbonisation of organic materials through an unknown proprietary method. The first ink recipe tested was the 10% EC ink but instead of using the Kuraray YP-80F, Enserv's Super Carbon was substituted in using the same mass and keeping the rest of the recipe the same. The CV curves obtained from this 10% EC Super Carbon are shown in figure 5.6. As the limitations of the electrolyte are already known from previous tests on the Kuarary the CV curves shown are only showing a 1V range between -0.5V and 0.5V far away from any voltages that could make the aqueous electrolyte split and form redox peaks in the CV curve that could disrupt the area calculations for capacitance. Because of this both the Super Carbon and the Kuraray YP-80F electrodes graph will be displayed. The CV curves of this material at the 1V potential window, in figure 5.7 show some rectangular shaped CV curves up until 100mV/s where the shape once again starts to become more of an oval with a point.

The average specific capacitance calculated using the areas of these curves is 79.63F/g when tested at 10mV/s.

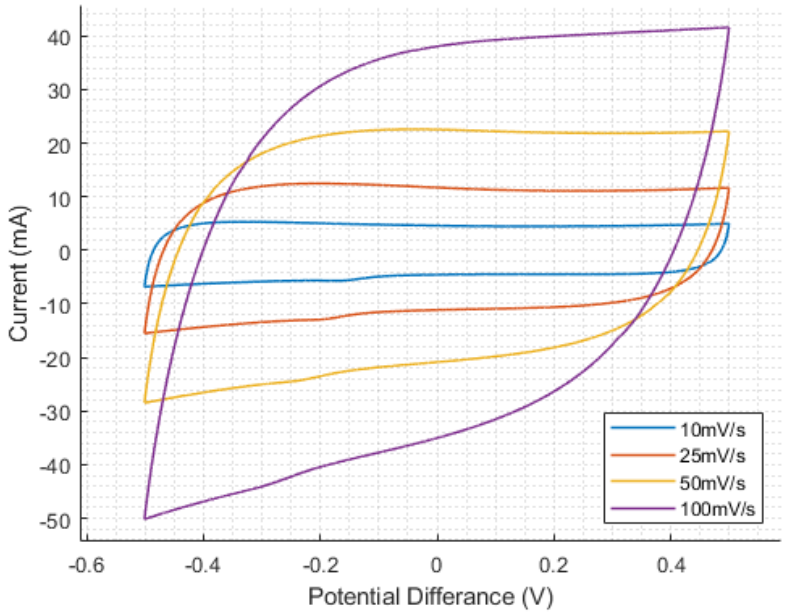

FIGURE 5.6:
CV curve of the 10% EC electrode using Super Carbon printed on nickel at varying scan rates with a -0.5V to 0.5V voltage window

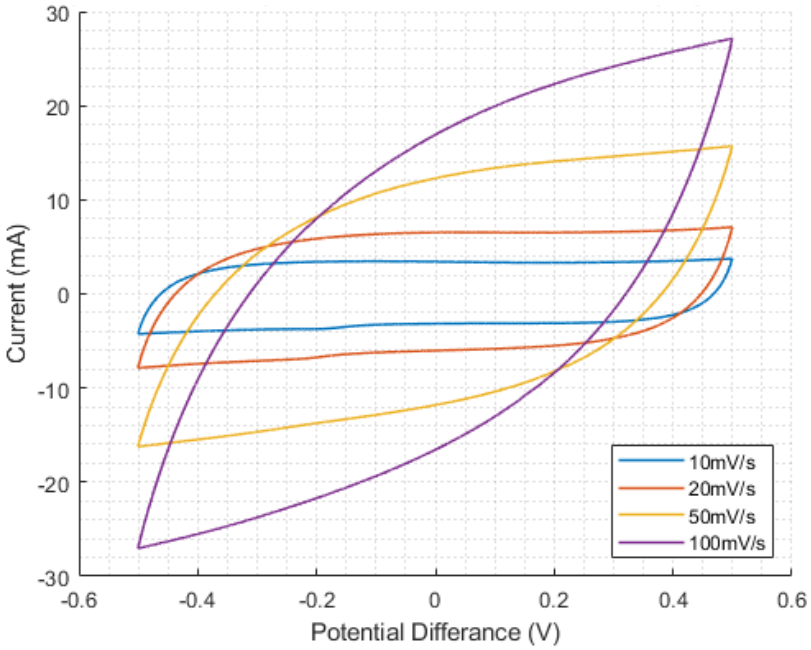

FIGURE 5.7:
CV curve of the 10% EC electrode using Kuraray YP-80F activated carbon printed on nickel at varying scan rates with a -0.5V to 0.5V voltage window

Multiple GCD graphs at varying currents for the 10% EC Super Carbon electrode carbon are shown in figure 5.8. Again, these GCD curves only go between -0.5V and 0.5V as to not let the electrolyte intervene in just the material testing. The GCD graph displays a triangular looking plot. The voltage jump evidently jumps a lot higher at higher currents. The voltage jumps for this GCD plot are shown in figure 5.9. Plotted against the specific currents at both 0.5V and -0.5V. the voltage drops at high and low voltage are both very similar and therefore the ESRs achieved, that are directly proportional to the gradients on this graph, are 1.93Ωand 1.94Ω respectively. The coulombic efficiencies are plotted against the specific current densities of this 10% EC Super Carbon electrode in figure 5.10. It shows as the current density increases the coulombic efficiencies decreases. The coulombic efficiency starts at 95.8% at 1.4A/g and ends at 89.6% at 13.8A/g.

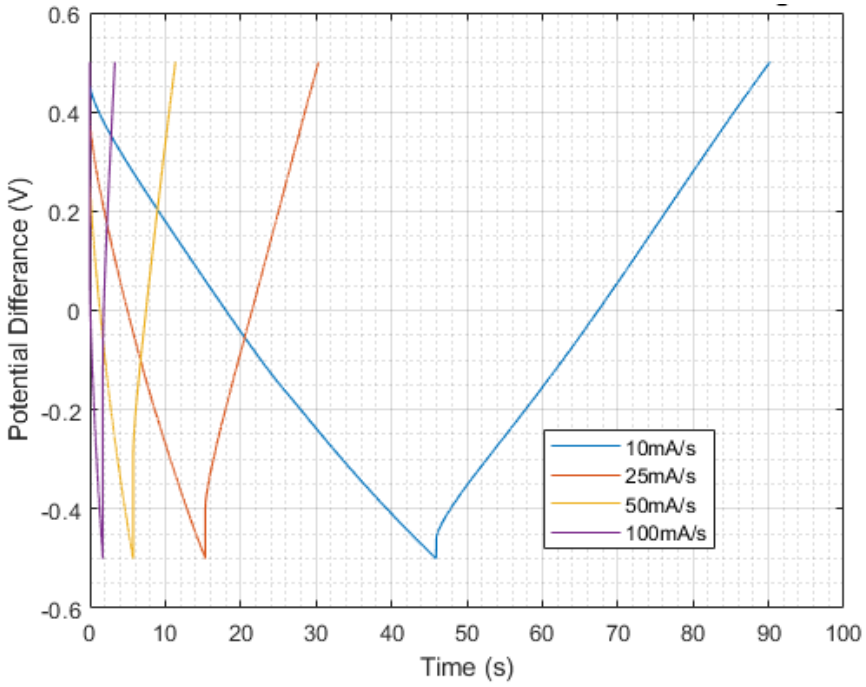

FIGURE 5.8:
GCD plot of the 10% EC electrode using Enserv's Super Carbon printed on nickel at multiple current densities

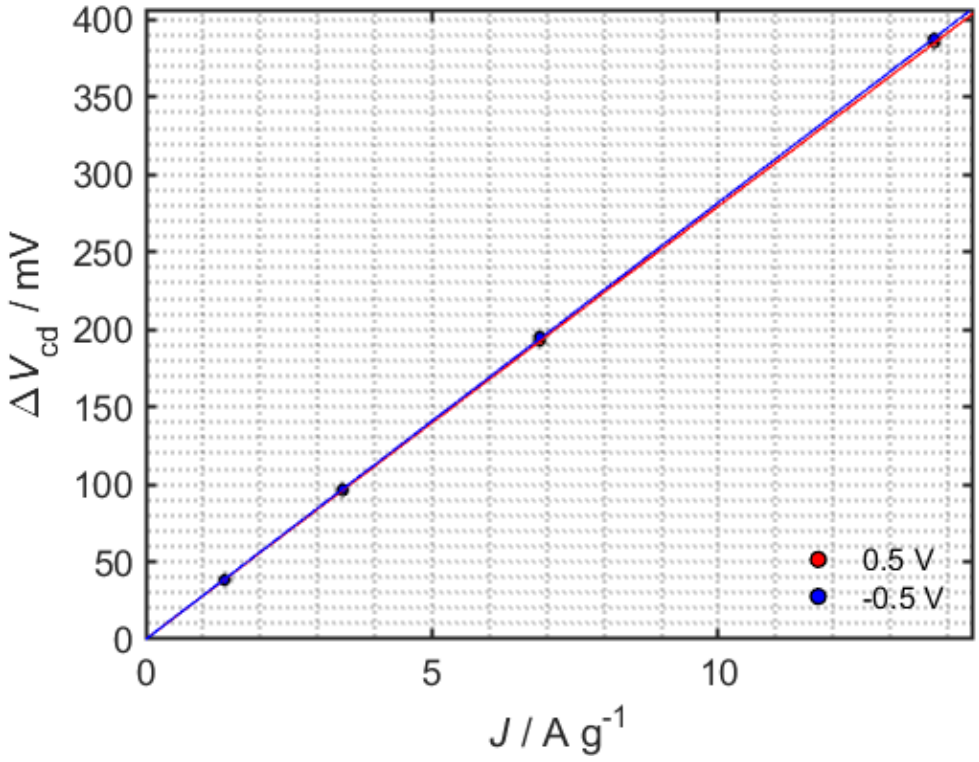

FIGURE 5.9:
Voltage drops at both minimum and maximum voltages plotted against specific currents for the 10% EC electrode using Enserv's Super Carbon

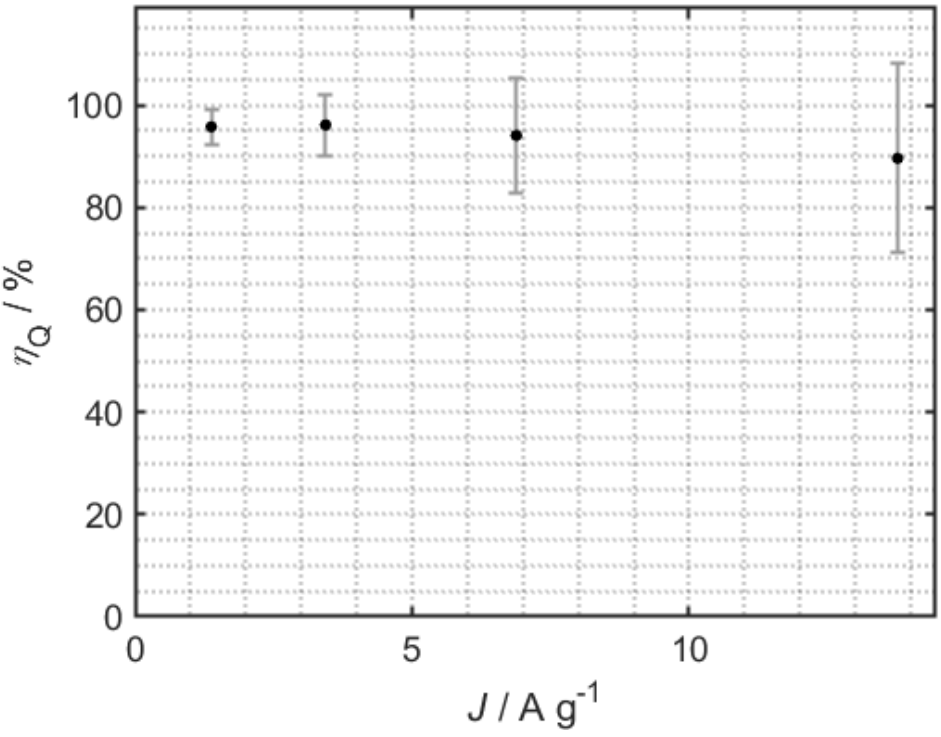

FIGURE 5.10:
Coulombic efficiency vs specific current of the 10% EC Enserv Super Carbon ink on a nickel substrate

The specific capacitances calculated by the GCD testing of the 10% EC ink made with Enserv's Super Carbon is shown in Figure 5.11 and are plotted against the current density during testing. The maximum capacitance reached was 82.7F/g at 1.4A/g which is considerably better than the maximum performance of the Kuraray YP-80F carbon with the same recipe. Like the previous specific capacitance Vs specific current graphs shown in this report the capacitances do decrease as the currents increase, however the capacitances in this figure are all considerably higher reaching a minimum capacitance of 41.3F/g at 13.8A/g, which again compared to previous results is considerably higher.

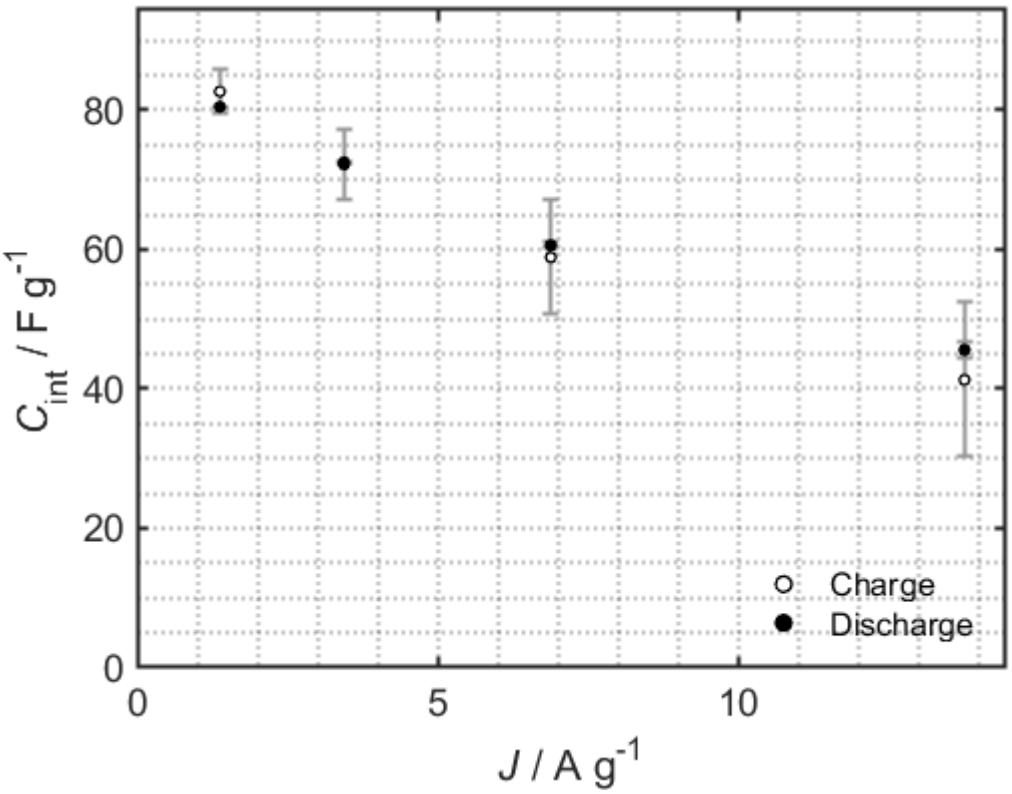

FIGURE 5.11:
Specific capacitance vs specific current of the 10% EC ink on a nickel substrate

The EIS plots for this electrode are shown in figure 5.12. It shows an average ESR of 1.4Ω. it has a slight semicircle in the starting high frequency region until the graph hits the 45^{O} angle and continues at this 45^{O} angle throughout the high frequency region.

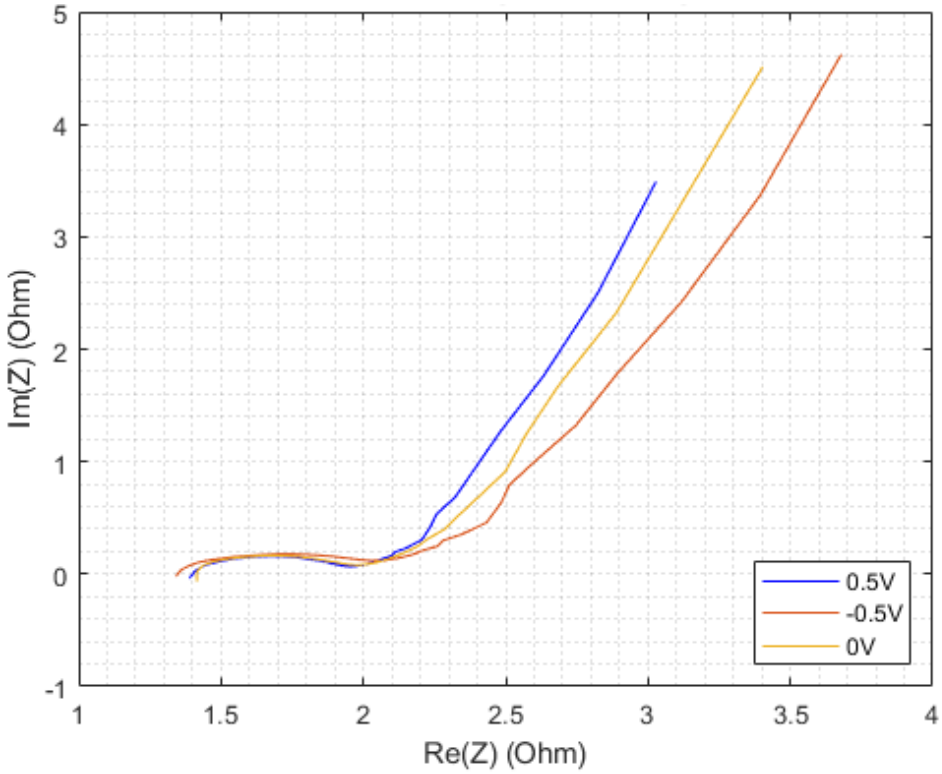

FIGURE 5.12
EIS plot of the 10% EC electrode using Enserv's Super Carbon printed on nickel

5.3 Discussion of Enserv's Super Carbon characterisation

The first and main conclusion from the preliminary characterisation of Enserv's Super Carbon is that the carbon particles are poorly sorted compared to Kuraray's YP-80F carbon meaning that there is a larger range of particle sizes in Enserv's Super Carbon mixture compared to Kuraray's carbon. As stated previously, the way that the carbons are sorted can affect the density of the electrode as it impacts on how the carbon particles are packed. With poorer sorting the density increases as the smaller particles sits in the interstitial spacing between the larger carbon particles. The fact that larger carbon particles are in the mix also indicates an increase in density as all of the volume form the larger grains would be carbon whereas if smaller particles were used this volume would be filled with both the smaller carbon particles and the interstitial spaces between them. However in supercapacitors, it is possible for the grains to be too big as the electrolyte may not be able to fully infiltrate the whole grain leaving a centre portion of the carbon to be dead mass that isn't used as a supercapacitor

material. The Particle size analysis of this carbon showed that there were some grains that were in the order of tens and even hundreds of microns meaning that there were some particles that had a diameter of around 100μm. Given that the intended printing thickness was 24μm the larger grains within the carbon mix could cause faults in the printing because the bar would carry the larger grains with it and cause lines on the print. However, these lines were not seen in any of the printed electrodes. One possible explanation for this was because the ink itself was mixed using a ball mill which could have broken up the larger carbon particles while mixing the carbon with the rest of the ink.

5.4 Discussion of electrochemical performance of Enserv's Super Carbon Electrodes

The results collected to date suggest that the overall performance of the Super Carbon is very promising. The first thing to note is that the specific capacitances measured were considerably higher than the Kuraray YP-80F carbon, the highest specific capacitance shown by Enserv's Super Carbon was 82.7F/g at 1.4A/g. The CV curves collected using the 10% EC ink using Enserv's carbon shows larger areas and more rectangularly shaped curves and the higher currents reached than that of the 10% EC Kuraray sample. What is very noticeable is that at higher voltage scan rates the rectangular supercapacitor like shape is maintained using Enserv's Super Carbon compared with the Kuraray which started to round off into a pointy oval, this suggests an increase in specific capacitance and overall coulombic efficiency in Enserv's Super Carbon electrode. The GCD performance was also rather promising, it showed some very triangular plots which indicate decent performance with relatively small voltage drops at the higher and lower limits. These voltage drops were plotted with the current densities of the tests and were found to be approximately equal for both the upper and lower limit. Also, these plots were all very linear indicating that the resistance of the electrode did not change with higher current densities. This is also shown in figure 5.10 illustrating the columbic efficiencies of this electrode. It shows the columbic efficiencies of the 10% EC ink electrode using Enserv's Super Carbon being somewhat stable even at higher currents with the highest current tested reaching 89.6% at 13.8A/g. This is comparatively high when compared to any of the coulombic efficiencies at higher currents for any Kuraray carbon electrode. This performance at higher currents is also shown in figure 5.11 which shows the specific capacitances of the electrode compared to the current it was tested at. It is shown that the capacitance of the Enserv Super Carbon electrode does decrease at higher currents like all the

other electrodes tested however it does not decrease as much as the Kuraray samples and the Super Carbon electrode ends on 41.3F/g at 13.8 A/g which a good result in comparison to the Kuraray sample in figure 4.21 that has a capacitance of 23.5F/g at 13.8A/g. The EIS plot for this electrode shown in figure 5.12 can possibly help explain the increase in performance of the electrode created using Enserv's Super Carbon. The starting equivalent series resistance shown in this figure has an average of 1.4V. This is less than any of the Kuraray electrodes' ESRs therefore the reduced resistance may cause the increase in performance. The EIS plots of the Enserv Super Carbon electrodes compared to the Kuraray EIS graph using the same 10% EC recipe has considerably less evidence of a semicircle at the beginning high frequency region indicating that there was less resistance due to surface interference. Also, what is seen in the Kuraray graphs is that in this semicircle region in the plots semi circles deviate depending on voltage which infers that the surface resistance in this section of the graph was proportional to charge transfer which could harm the performance of the electrode at high currents. This deviation implies that correlation with charge transfer was not present in the electrode made with Enserv's Super Carbon.

In conclusion, Enserv's Super Carbon performed very well compared to the Kuraray YP-80F activated carbon tested using the same recipe. This is shown by the maximum specific capacitance of 82.7F/g at 1.4A/g. It is also shown that even at higher current densities the performance that decreased considerably using Kuraray YP-80F while it did not decrease as much using Enserv's Super Carbon.

CHAPTER 6. Conclusion and Future Research

6.1 Conclusion

The aim of this project was to explore the formulation of activated carbon inks for supercapacitor applications, in particular as anode for a asymmetric supercapacitor design. The research focused on the use of ethyl cellulose as binder at varying concentrations (3 levels: 20%, 10%. 5%), aiming to identify an optimum concentration. Finally, Enserv Super Carbon, was preliminary tested as alternative to the Kuraray YP-80F activated carbon, which was used in the optimisation study, to compare the performances of these carbons.

A first conclusion from optimisation study was evidence that a 10% concentration of EC appears to provide the best performance with a specific capacitance of 62.3F/g at 1.4A/g. This performed better than the 20% (adopted in previous studies for Enserv) and vastly better than 5%. In theory, a decrease in binder material would lead to higher active material and therefore potentially increase the performance of the electrode in general. The results were that the halving of the binder from 20% to 10% led to a performance improvement of 62.3F/g at 1.4A/g for 10% versus a 28.9F/g at 1.0A/g for 20%. Also, in terms of specific capacitance at higher currents and columbic efficiency the 10% outperformed the 20% formulation. Specific capacitance decreased with higher current with 23.5F/g at 13.8A/g for 10% and 16.55F/g at 9.9A/g. Higher currents resulted also in a modest decrease in columbic efficiency, in particular 10% decreased from 95% at 1.38A/g to 81% at 13.76A/g and 20% from 5% at 0.99A/g to 89% at 9.93A/g

The 5% concentration of EC resulted in the lowest performance, with only 17.4F/g at 1.9A/g, It was hypothesised that this concentration was inadequate causing a lack of internal adhesion and contact (among particles themselves and the substrate) leading to higher internal resistance.

It is further important to underline that the results for the 10% concentration of EC are in line with best capacitance observed in literature with the same YP-80F activated carbon, but other polymers. It is evident therefore that EC appears a potential polymer (adopting DAA as solvent) combining performance with ease of management/manufacture.

Early testing of novel Enserv Super Carbon instead of the Kuraray YP-80F (that was tested in the binder content optimisation) showed very promising results, better than YP-80F

within same formulation. The starting capacitance at the lowest current density was 82.7F/g and a coulombic efficiency of 95.8% at 1.4A/g which compared to any other recipe tested in this project was considerably better. The 10% EC electrode that was made from Kuraray YP-80F lost capacitance and efficiency at higher current densities, the electrodes that were made form Enserv's Super Carbon ended up with a capacitance of 41.3F/g and a coulombic efficiency of 89.6%, both at 13.8A/g. so there was still a decrease in both capacitance and efficiency however, this decrease was considerably smaller than the decrease observed with the electrodes made with Kuraray YP-80F.

6.2 Future Work

The primary work in this thesis was determining how the decrease of binder in the ink recipe would change the performance of the electrode material. Future work on the ink recipe could include:

- Control of solvent addition and rheology testing of the ink
- Changing ratio of conductive carbon / active material testing
- Printing control (print thickness/roughness)

Part of this thesis was to show preliminary results for Enserv's Super Carbon, a high surface area activated carbon produced from a proprietary confidential method. This carbon displayed excellent results compared to the industrially available Kuraray YP-80F however, as this work was only the preliminary research there are still many more tests to perform using Enserv's Super Carbon including:

- Raman analysis of the Super carbon
- BET surface are analysis of Enserv's Super Carbon
- Testing of Enserv's Super Carbon at higher current densities
- Particle size-controlled testing of Enserv's Super Carbon using sieves

As this research is an early step in creating a manufacturing line that creates supercapacitors there are also many next steps that can be explored working towards the scaled-up production of activated carbon electrodes some of these steps could include:

- Higher surface area electrode testing
- Testing of symmetric Carbon/Carbon electrode

- Testing of Asymmetric Carbon/Metal oxide electrode
- Testing mixing techniques for larger volume ink recipes

It is hoped that this future work will help optimise supercapacitors in future energy storage solutions.

CHAPTER 7: Bibliography

[1] Partridge J, Abouelamaimen D. The Role of Supercapacitors in Regenerative Braking Systems. Energies [Internet]. 2019 [cited 29 September 2022];12(14):2683. Available from: https://doi.org/10.3390/en12142683

[2] Choi N, Chen Z, Freunberger S, Ji X, Sun Y, Amine K et al. Challenges Facing Lithium Batteries and Electrical Double-Layer Capacitors. Angewandte Chemie International Edition [Internet]. 2012 [cited 29 September 2022];51(40):9994-10024. Available from: https://doi.org/10.1002/anie.201201429

[3] Muzaffar A, Ahamed M, Deshmukh K, Thirumalai J. A review on recent advances in hybrid supercapacitors: Design, fabrication and applications. Renewable and Sustainable Energy Reviews [Internet]. 2019 [cited 29 September 2022];101:123-145. Available from: https://doi.org/10.1016/j.rser.2018.10.026

[4] Choudhary N, Li C, Moore J, Nagaiah N, Zhai L, Jung Y et al. Asymmetric Supercapacitor Electrodes and Devices. Advanced Materials [Internet]. 2017 [cited 29 September 2022];29(21):1605336. Available from: https://doi.org/10.1002/adma.201605336

[5] Demarconnay, L., Raymundo-Piñero, E. and Béguin, F., 2022. A symmetric carbon/carbon supercapacitor operating at 1.6V by using a neutral aqueous solution. [online] Available at: http://dx.doi.org/10.1016/j.elecom.2010.06.036

[6] Béguin, F., Presser, V., Balducci, A. and Frackowiak, E., 2014. Carbons and Electrolytes for Advanced Supercapacitors. Advanced Materials, [online] 26(14), pp.2219-2251. Available at: https://doi.org/10.1002/adma.201304137

[7] Hong, M., Lee, S. and Kim, S., 2002. Use of KCl Aqueous Electrolyte for 2 V Manganese Oxide/Activated Carbon Hybrid Capacitor. Electrochemical and Solid-State Letters, [online] 5(10), p.A227. Available at: https://www.scopus.com/record/display.uri?eid=2-s2.0-0036795894&origin=inward&txGid=9efdf335b9fc0cdaab0d00e98a6dd3ae

[8] Raymundo-Piñero, E., Kierzek, K., Machnikowski, J., & Béguin, F. (2006). Relationship between the nanoporous texture of activated carbons and their capacitance properties in different electrolytes. *Carbon*, *44*(12), 2498-2507. doi: 10.1016/j.carbon.2006.05.022

[9] Brousse, T., Toupin, M. and Bélanger, D., 2004. A Hybrid Activated Carbon-Manganese Dioxide Capacitor using a Mild Aqueous Electrolyte. Journal of The Electrochemical Society, [online] 151(4), p.A614. Available at: https://www.scopus.com/record/display.uri?eid=2-s2.0-2042515590&origin=inward&txGid=d4ade8bd497fd32ebe920583e2747ad2

[10] Khomenko, V., Raymundo-Piñero, E. and Béguin, F., 2006. Optimisation of an asymmetric manganese oxide/activated carbon capacitor working at 2V in aqueous medium. Journal of Power Sources, [online] 153(1), pp.183-190. Available at: https://reader.elsevier.com/reader/sd/pii/S0378775305005744?token=CF5F9783752FCB21EA0D2D0AA88BB9AA49B7D5A38A818BB61334B05F655950FC02C9B34551BBA4F0702268AF04AC6585&originRegion=eu-west-1&originCreation=20220126200521

[11] Gamby, J., Taberna, P., Simon, P., Fauvarque, J., & Chesneau, M. (2001). Studies and characterisations of various activated carbons used for carbon/carbon supercapacitors. *Journal Of Power Sources*, *101*(1), 109-116. Available at: https://doi.org/10.1016/S0378-7753(01)00707-8

[12] Kim, T., Yi, S., & Chun, S. (2020). Electrophoretic deposition of a supercapacitor electrode of activated carbon onto an indium-tin-oxide substrate using ethyl cellulose as a binder. *Journal Of Materials Science &Amp; Technology*, *58*, 188-196. doi: 10.1016/j.jmst.2020.03.072, from https://doi.org/10.1016/j.jmst.2020.03.072

[13] Shrestha, M., Amatya, I., Wang, K., Zheng, B., Gu, Z., & Fan, Q. (2017). Electrophoretic deposition of activated carbon YP-50 with ethyl cellulose binders for supercapacitor electrodes. *Journal Of Energy Storage*, *13*, 206-210. doi: 10.1016/j.est.2017.07.015, from https://doi.org/10.1016/j.est.2017.07.015

[14] Li, Y., Cao, L., Qiao, L., Zhou, M., Yang, Y., Xiao, P., & Zhang, Y. (2014). Ni–Co sulfide nanowires on nickel foam with ultrahigh capacitance for asymmetric supercapacitors. *J. Mater. Chem. A*, *2*(18), 6540-6548, from https://doi.org/10.1039/C3TA15373H

[15] Zhang, H., Zhang, X., & Ma, Y. (2022). Enhanced capacitance supercapacitor electrodes from porous carbons with high mesoporous volume. Retrieved 6 September 2022, from http://dx.doi.org/10.1016/j.electacta.2015.10.089

[16] Linear Sweep Voltammetry/Cyclic Voltammetry. (2022). Retrieved 7 September 2022, from https://www.basinc.com/manuals/EC_epsilon/Techniques/CycVolt/cv

[17] Yu, M., Lu, Y., Zheng, H., & Lu, X. (2018). New Insights into the Operating Voltage of Aqueous Supercapacitors. *Chemistry - A European Journal*, *24*(15), 3639-3649. doi: 10.1002/chem.201704420, from https://doi.org/10.1002/chem.201704420

[18] KURARAY COALTM YP Series. (2022). Retrieved 7 September 2022, from https://www.calgoncarbon.com/app/uploads/YP-brochure-draft_final_08_2019.pdf

[19] Platek, A., Nita, C., Ghimbeu, C., Frąckowiak, E., & Fic, K. (2020). Electrochemical capacitors operating in aqueous electrolyte with volumetric characteristics improved by sustainable templating of electrode materials. *Electrochimica Acta*, *338*, 135788. From https://doi.org/10.1016/j.electacta.2020.135788

[20] Kostoglou, N., Koczwara, C., Stock, S., Tampaxis, C., Charalambopoulou, G., & Steriotis, T. et al. (2022). Nanoporous polymer-derived activated carbon for hydrogen adsorption and electrochemical energy storage. *Chemical Engineering Journal*, *427*, 131730. From https://doi.org/10.1016/j.cej.2021.131730